CHALMERS
UNIVERSITY OF TECHNOLOGY

Experimental studies on Chemical-looping combustion in a packed-fluidized bed

Effects of packing type and bed height

Master's thesis in Sustainable energy systems

YUKARI TSUJI

Department of Space, Earth and Environment
CHALMERS UNIVERSITY OF TECHNOLOGY
Gothenburg, Sweden 2021

Master's thesis 2021

Experimental studies on Chemical-looping combustion in a packed-fluidized bed

Effects of packing type and bed height

YUKARI TSUJI

CHALMERS
UNIVERSITY OF TECHNOLOGY

Department of Space, Earth and Environment
Division of Energy technology
Chalmers University of Technology
Gothenburg, Sweden 2021

Experimental studies on Chemical-looping combustion in a packed-fluidized bed
Effects of packing type and bed height

YUKARI TSUJI

Supervisor: Nasrin Nemati, Department of Space, Earth and Environment
Examiner: Magnus Ryndén, Department of Space, Earth and Environment

Master's Thesis 2021
Department of Space, Earth and Environment
Division of Energy technology
Chalmers University of Technology
SE-412 96 Gothenburg
Telephone +46 31 772 1000

Typeset in LaTeX
Printed by Chalmers Reproservice
Gothenburg, Sweden 2021

Experimental studies on Chemical-looping combustion in a packed-fluidized bed: Effects of packing type and bed height

YUKARI TSUJI
Department of Space, Earth and Environment
Chalmers University of Technology

Abstract

Chemical Looping Combustion (CLC) is a technology that can be used as a gas separation technology for Carbon Capture and Storage (CCS). Compared to other alternatives, it is considered to have lower investment and operational costs per amount of CO_2 captured. CLC utilizes fuel and air reactors where the use of fluidized beds can be an advantage. For industrial applications, fuel conversion rates for higher bed heights need to be improved. One possible solution could be to add packings in the reactors to inhibit bubble growth and possibly increase the fuel conversion rate by increasing the mass transfer rate.

This project investigated possible improvements of fuel conversion rate in a packed fluidized bed for Chemical Looping Combustion(CLC). Two types of fuel, Syngas and CO, were tested with two different types of packings, RMSR and Hiflow® ring, as well as without packings. All tests were conducted with a small laboratory scale reactor and bed heights between 10 and 60 cm.

The results show that the fuel and CO conversion rates increase as the bed height increases. This could be due to spouting or insufficient fluidization when having a lower bed height, leading to a shorter reaction path. The relative increases in conversion rate are the highest for lower bed heights. However, for taller beds the conversion rates are above 96 % without packings and approach 100 % with. A fluidized bed equipped with RMSR has the best overall fuel conversion rates but use of packings in general showed an improvement when compared to the experiments without them. For higher beds without packings there were some observations indicating large bubble formation. The lack of similar observations when packings were used could indicate that the they are inhibiting the formation of large bubbles as intended. In conclusion, the use of packings in a fluidized bed for CLC seems to increase the the fuel conversion rate, possibly through the inhibition of bubble growth.

Further studies, with taller beds as well as with other packings with different geometries and materials, under different operating temperatures and pressures, are recommended. Study of bubble formation and inhibition with packings in a fluidized bed can also contribute to the understanding of the effect of packings for bubble inhibition and hence the rates of mass transfer and fuel conversion.

Keywords: Packed-fluidized bed, Chemical-looping combustion, CCS, metal random packing, fuel conversion

Acknowledgements

First of all, much appreciation goes to my supervisor, PhD student Nasrin Nemati, who has been supportive, guiding, patient and understanding, as well as to my examiner, Magnus Rydén, who gave me this great learning opportunity. Both have been warm-welcoming from day one and have enthusiastically answered all my questions. I am honoured to be able to take part in a project which can potentially have a significant effect on our future.

I also want to show my gratitude to research engineers Johannes and Rustan at the M7 lab. They have shown nothing but support and have aided me in my laboratory work.

I also want to thank for my partner Lars, for his various support and for always being there for me. Many thanks also go to my grandmother. She is my role model and taught me to always try learning new things and to not be afraid of challenges.

Finally, I would also like to thank all the classmates, teachers and supervisors who have helped me while studying at Chalmers. It was not always easy but thanks to everyone I have been able obtain important experiences, knowledge, strength and the determination to tackle any future obstacles or challenges in my life.

Yukari Tsuji, Gothenburg, 01 2021

Contents

List of Figures

List of Tables

Nomenclature

Constant

g	The gravitational force	$9.82\,m/s^2$
R	The gas constant	$8.314\,JK^{-1}mol^{-1}$

Variables

P_{atm}	Ambient pressure	kPa
P_{dp}	Pressure drop over distributor plate	kPa
P_{WB}	Pressure drop of bed	kPa
ΔH	The lower heating value	J/mol
ΔP	Pressure drop	Pa
ΔP_{bed}	Pressure drop of bed	kPa
$\dot{n}$	Molar flow rate	mol/s
ϵ	Voidage	$-$
Γ	Gas yield	$-$
ω	Mass based Ilmenite conversion rate	g
ρ_g	Gas density	kg/m^3
ρ_p	Solid density	kg/m^3
A	Cross-sectional area	m
G_b	Bubble phase flow rate	m/s
H	Bed height	m
k_{eq}	Equilibirum constant	$-$
m	Ilmenite mass	g
m_{ox}	Fully oxidized Ilmenite mass	g
M_o	Oxygen molar mass	kg/mol
m_{tot}	Total mass	g
m_{void}	Void mass	g
P	Pressure	kPa
q	Total flow rate	$nlpm$
T	Tempareture	K or $^\circ C$

t	Time step	s
U	Fluid velocity	m/s
U_g	Superficial gas velocity	m/s
X	Fraction of transfered oxygen and fully oxidized Ilmenite mass	g
Y	Correction factor for two phase theory	$-$
μ	Viscosity of liquid	$Pa\ s$
$_p$	Sieve size of bed particle	m
u_{mf}	Superficial minimum fluidization gas velocity	m/s
x_{sv}	Surface-volume diameter	m

Other Symbols

Ar	Archimedes number
Re_{mf}	Reynolds number at minimum fluidization

1
Introduction

Reducing CO_2 emissions is an urgent issue when mitigating the environmental effects expected from global warming. This cannot be achieved solely through political and social efforts. Technological means are also required if the stated targets of organizations such as the Intergovernmental Panel on Climate Change (IPCC) are to be met. One of the many methods used to decrease CO_2 emissions is Carbon Capture and Storage (CCS). CO_2 is separated from other gases produced during combustion processes, captured and then stored in a manner so that it cannot be released into the atmosphere, for example in an underground geological formation.[1] This way, the emissions from the combustion of fossil fuels are contained and zero emissions can be achieved. If fuels that are low carbon, such as biomass or biogas, are utilized, even net negative emissions can be expected over a long time span.[1] According to some models, enabling negative emissions is currently the only way to achieve the stated environmental goals.[2] These technologies are obviously not complete solutions to the problem but they will contribute to the mitigation efforts and increase the available time when looking for more fundamental solutions and adjusting society so that lower CO_2 emissions become a reality. The viability of the concept has been recognized and many CCS projects have been launched all over the world in the past decades. [3]

1.1 CLC for CCS

There are several gas separation technologies such as adsorption, amine scrubbing and oxy-fuel combustion. Each technology has strengths and weaknesses in terms of cost, efficiency and operational range.[4] Due to the exhaust mainly being CO_2 and water vapour, CLC is one of the technologies that simplifies the separation of CO_2 from other gases formed during combustion. A fundamental principle of CLC is the utilization of air and fuel reactors and a simplified schematic of it is shown in figure 1.1. A metal oxide (Me_xO_y) acts as an oxygen carrier between the reactors and a carbon based fuel reacts with oxygen in the fuel reactor. This allows for two separated outlet gas flows of oxygen depleted air, and CO_2 and H_2O. The H_2O can easily be separated from the CO_2 by condensation, therefore there is no need for a complex separation system.[5]

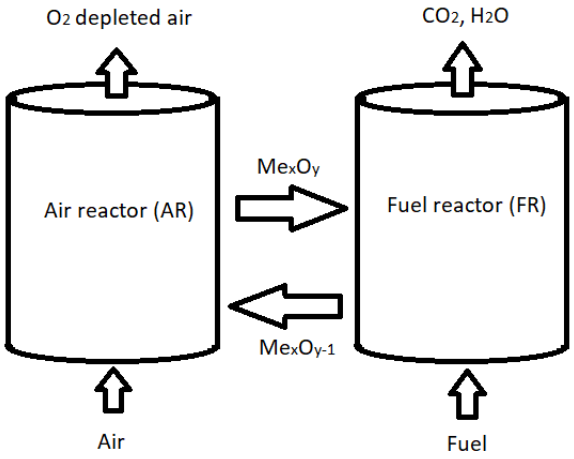

Figure 1.1: CLC simplified schematic

Initially, CLC with gas fuels have been the most studied but due to the ease of transport and cost the most used fuel today is solid and the development efforts of CLC designed for both gas and solid fuels have been intensified in recent years.[6] Many different designs for CLC reactors have been suggested and studied. One design that has gained traction is similar to the general concept of a Circulating Fluidized Bed (CFB) and is shown in figure 1.2.[6] An interconnection between the air and fuel reactors allow a continuous transfer of oxygen carrier particles while the outlet flows are completely separated. This design can be applied even with solid fuels but an adaptation of the fuel reactor is required due to the intermediate reaction involving char.[6]

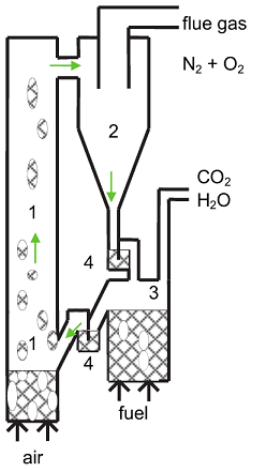

Figure 1.2: Example of CLC design [6]

The conventional gas separation methods result in a relatively high energy penalty in comparison to this method. Furthermore, CLC can be implemented in the existing systems, bringing a relatively low investment cost. One specific case calculation even shows that the total cost for CCS with solid fuel CLC is estimated to be 20 €

per tonne of CO_2 [7]. Many CLC experiments have been run on small scale units in the range of 0.3 to 100 kW over a total of 11,000 hours, with various different types of fuels and oxygen carriers[8]. Some of the challenges that must be faced when up-scaling the technology have become apparent. For instance, selection of suitable oxygen carrier materials, improvement of gas conversion rate in fuel reactor, downstream treatment and bio fuels. [6][9]

1.2 Fluidized bed for CLC

As previously mentioned fluidized beds are typically used in the CLC design due to the many advantages that fluidization brings. Fluidization particles act as oxygen carriers in the bed. Extensive research has been done regarding the selection of particle types for CLC, based on criteria such as reactivity, fuel conversion rate and chance of agglomeration, as well as monetary cost, environmental cost and safety.[10] A conclusion as to what is the optimum choice of bed particle is yet to be seen, but the most frequently used oxygen carriers in pilot plants have been $FeTiO_3$/ilmenite, CuO, Fe_2O_3 and iron ore[6][10].

Undesired large bubbles can form during fluidization, hindering effective solid-gas mass transfer. The phenomena increases in likelihood in relation to a higher gas velocity and higher pressure drop due to bed height. This is one of the apparent challenges when scaling up for commercialization[8]. Aronsson et al [11][12] have suggested that the limiting factor for the fuel conversion of CLC in a fluidized bed can be the mass transfer rather than the chemical reaction. This led to the idea of adding packings with the intention of eliminating the large bubbles that occur. Packings are often used in chemical separation processes to increase contact surfaces and are available in different shapes and materials. The experiments resulted in increased fuel conversion rate in comparison to the case without packings and concluded that packings can possibly enhance the gas−solids mass transfer rate. [13] This shows a potential improvement in the fuel reactor for CLC when utilizing packings. However, this study is limited to two kinds of packings and low bed heights in the range of 2 cm to 25 cm. The higher bed with higher pressure drop increases the risk of slugging and bypassing, which is the reason why higher bed heights need to be further investigated. As an improvement of gas-solid mass transfer in larger scale fuel reactors can be a key to commercialization [8][14], more research also needs to be done with different types of packings.

1.3 Aim

The aim of the project is to investigate the effects of different types of packings, namely Hiflow® ring and RMSR, as they are yet to be tested in terms of fuel conversion rate for CLC in a fluidized bed reactor. Since the material of the packings is same, the geometrical form of the packings are likely to be the main cause of any difference in bubble inhibition between the two. The bed height is varied in a wide range from 10 cm to 60 cm, with increments decided by time constraints when

testing. Additionally, water-gas shift effect is investigated by testing two different types of gases: CO, and Syngas which consists of 50% CO and 50% H_2 and is similar to the composition of gasified biogas. These experiments are conducted in the hope that the findings will take us a step closer to up-scaling and industrial implementations.

1.4 Focus of the study and limitations

This study focuses on CLC fuel conversion rates in a fluidized bed reactor equipped with two different types of packings. The study is limited to fuel conversion rates in a reactor with gaseous fuel, therefore ash chemistry is not taken into account. The effects on conversion rates due to chemical reaction details are also not considered. Only the effects of packings and bed height are considered. The bed height is limited from 10 cm up to 60 cm due to limitations in reactor height and risk of spouting. Only Ilmenite is investigated as the bed particle, as earlier studies have proven it to be a valid oxygen carrier and that is the most important property for this project.

2

Theory

2.1 Fluidization

Fluidization is a phenomena where solids behave as if they are fluids when a gas flows through them, examples of the fluid-like behavior being light objects floating on the fluidized solid and solids having flow like properties. These properties provide advantages such as smooth continuous flow, quick and well mixing, enabling circulation of solids, high mass and heat transfer rate and easier handling compared to liquids. [15] Fluidization has many applications such as combustion, gasification, synthesis reactions, drying, coating and adsorption. [15]

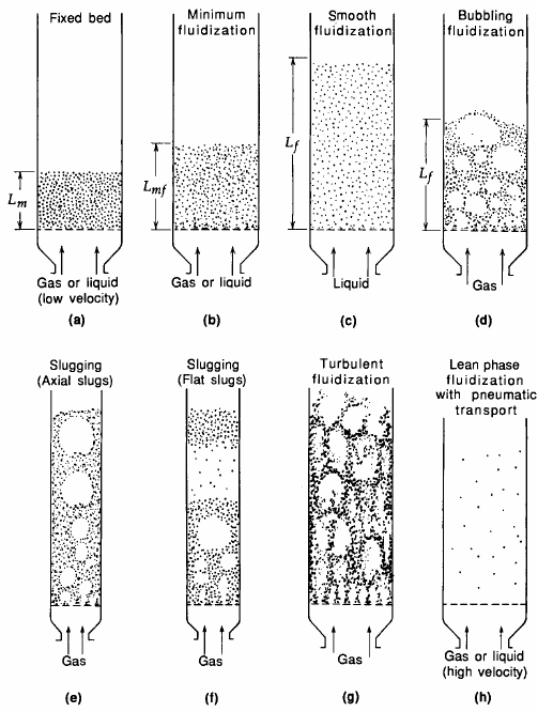

Figure 2.1: Fluidization state in a bed [15]

Intensive research regarding fluidization has been conducted by Kunii and O. Levenspiel. The state of fluidization is categorized as shown in figure 2.1. a) shows gas merely passing through the void space between particles since the drag force on the solids is smaller than the gravitational force at low velocities. This state is called a *fixed bed*. With increasing gas velocity, the net force on a particle becomes zero and

this is the state of minimum fluidization. The bed expansion starts occurring at this point and continues until it reaches maximum expansion at bubbling fluidization. When the bed particles are fine solids, the bubbles coalesce and form large bubbles as in figure 2.1 e) and can even cover the cross-sectional area as shown in f). This phenomena is called slugging and is often observed in a narrow, long beds. Another notable phenomenon is spouting. At high gas velocity, gas transports solid particles through the bed to the top as if it was a fountain and this can cause spillage of particles. By increasing the velocity further, turbulent fluidization where entrainment occurs, and equipping, for instance a cyclone, to collect entrained particles becomes a requirement in the case of continuous operation.[15] In the application of fluidized beds in CLC, bubbling fluidization is a desirable state as it is suitable for fine solids and gives uniform temperature distribution as well as enabling continuous operations.[15]

According to Geldart[16], the quality of fluidization is mostly influenced by the particle size and the size distribution, the fluid-solid ratio and the geometry of the bed. In the case of gas as a fluid, there is a classification of fluidization characteristics known as *the Geldart groups* where the particle types are divided into four groups depending on the density difference between the fluid (air at atmospheric pressure) and the solid. Ilmenite, which is used in this project, belongs to group B. This group contains particles with a mean size between 40 and 500 μm and a density in the range of 1.4 g/cm^3 to 4 g/cm^3. A property of group B is that the bubbling occurs at the same time as reaching minimum fluidizaiton and that the bubble size becomes larger as the bed height and gas velocity increase.[16] This group also tends to have moderate bed expansion as well as moderate solid and gas mixing. Spouting can happen at lower bed heights. [17]

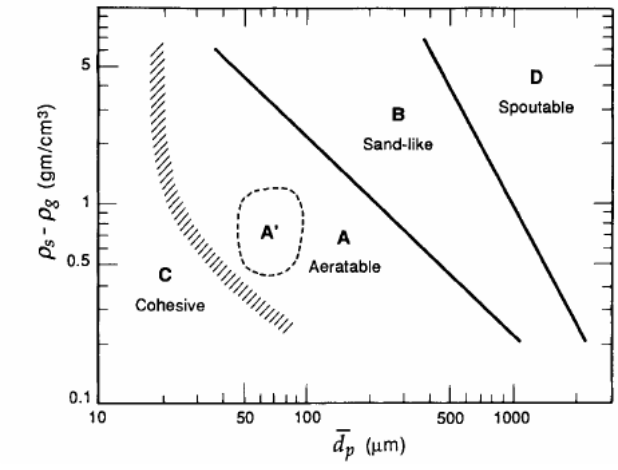

Figure 2.2: The Geldart group classification [16]

The motion of fluids in a fluidized bed caused by density differences is described by a dimensionless number called *Archimedes* number Ar as in equation 2.1 which is often used for conventional packed fluidized bed.

$$Ar = \frac{\rho_f(\rho_p - \rho_f)gx_{sv}^3}{\mu^2} \tag{2.1}$$

The Reynolds number at the minimum fluidization is given by the equation 2.2 [17] which is dependent on the minimum fluidization superficial velocity.

$$Re_{mf} = \frac{u_{mf}x_{sv}\rho_f}{\mu} \tag{2.2}$$

According to Rhodes[17], the gas velocity in a fluidized bed without packings can be theoretically obtained in two ways. The first way is to calculate it with the equation 2.3 which is obtained by equating the expression for pressure loss in a fluidized bed with the expression for pressure loss across a packed bed. But the voidage of the bed, which is a volume fraction occupied by voids, has to be calculated. Therefore the assumption needs to made that the voidage at the minimum fludization is the same as that of the voidage of the bed.

$$Ar = 150\frac{(1-\epsilon)}{\epsilon^3}Re_{mf} + 1.75\frac{1}{\epsilon^3}Re_{mf}^2 \tag{2.3}$$

where Ar, that comes from 2.1, and Re_{mf}, from 2.2[17], are inserted into the equation and u_{mf} is obtained.

Another method is to assume that the voidage of the bed as 0.4, which leads to:

$$Ar = 1406Re_{mf} + 27.3Re_{mf}^2 \tag{2.4}$$

This is similar to the empirically obtained Wen and Yu correlation 2.5[17]. This correlation is most suitable for particles with a size of less than 100 μm.

$$Ar = 1652Re_{mf} + 24.51Re_{mf}^2 \tag{2.5}$$

For larger particles, Baeyens and Geldart correlation can be used. 2.6 [17]

$$u_{mf} = \frac{(\rho_p - \rho_f)^{0.934}g^{0.934}x_p^{1.8}}{1110\mu^{0.87}\rho_f^{0.066}} \tag{2.6}$$

The gas velocity ranges are different for different Geldart groups, as equation 2.6 is dependent on the density difference between fluid and solid. Typical operational superficial gas velocity of a fluidized bed for Geldart group B is 0.5 to 3 m/s.[18] The minimum fludization velocity is almost equal to the bubbling fluidization velocity, and a velocity increase in the range of 0 to 0.3 m/s achieves it.[18] An increase of 0.3 to 2 m/s from the minimum fluidization velocity will reach a slugging state. An increase above 2 m/s is likely to cause a turbulent fluidization state.[18] However, other factors such as ambient pressure and temperature, can also have an effect. How these factors affect the minimum fluidization velocity also differs between the Geldart groups. [17]

Regarding packings in a fluidized bed, Sutherland et al [19] has investigated the effect of different packings. Key findings are that both packing size and particle to

packing diameter ratio affect minimum fluidization velocity and bed expansion. The ratio is dependent on the geometry and arrangement of packings, and roughness of both packing and bed particles. For smooth spherical packings the maximum ratio is 0.096 with spherical particles, and 0.055 with angular particles.

2.2 Pressure drop in a fluidized bed

In a conventional fluidized bed a pressure drop caused by frictional resistance through bed particles occurs. Figure 2.3 illustrates the relation between pressure drop and fluid velocity from a fixed bed state up to a bubbling fluidization state. Point A is where the minimum fluidization is initiated and the pressure drop of the bed is the highest. [17]

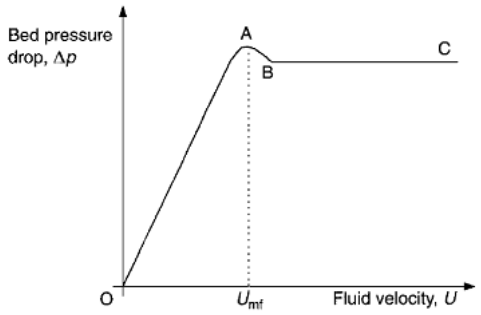

Figure 2.3: Pressure drop against fluid velocity for a packed fluidized bed [17]

The region between O and A is a fixed bed region where the pressure drop is proportional to the fluid velocity and is linear. The Ergun equation 2.7 shows the relation between the pressure drop and the fluid velocity in this region [17] and this equation is the basis for the equation describing the superficial minimum fluidization velocity (equation 2.3).

$$\frac{-\Delta P}{H} = 150\frac{\mu U}{x_{sv}^2}\frac{(1-\epsilon)^2}{\epsilon^3} + 1.75\frac{\rho_f U^2}{x_{sv}}\frac{(1-\epsilon)}{\epsilon^3} \tag{2.7}$$

Equation 2.8 is valid only for the fluidization region between B and C. [17] In this region, the pressure drop is theoretically equal to the effective mass over cross-sectional area at a given height, and is relatively constant since the increasing velocity has less effect on the pressure due to bed expansion and the flow of gas through the solids. [20]

$$\Delta P_{bed} = h(1-\epsilon)(\rho_P - \rho_g)g \tag{2.8}$$

The pressure drop is thus dependent on the density difference between fluid and solid, as well as voidage in relation to the bed's cross-sectional area for a conventional fluidized bed.

In this project, not only bed particles but also packings are placed in the bed. Experiments by Donsi et al [21], with coarse spherical packings set in the column and Geldart group A and B particles, made observations that the pressure drop increased with packings when and the solid mass remained unchanged. Aronsson et al[12] has investigated two scenarios: one where the mass remains the same and another where the bed height remains the same. For the first scenario the findings were that the pressure drop in a reactor is higher when both packings and bed particles are present, compared to bed particles alone. For the second scenario it was found that the pressure drop is higher without packings when the bed heights are equal. This study also shows that the pressure drop is almost zero when only packings are in the bed. Experiments with a rectangular fluidized bed with packings conducted by Song et al [22] suggest that the pressure drop is caused mostly by the particle hold-up, the friction between gas and packings and between bed particle and packing. K.G. Allen et al [23] have conducted experiments on the effects on bed pressure in a cold flow for packings with both spherical and non-spherical geometries, and both random and structural placement. The arrangement of packings for non-spherical packings have a significant impact on the friction factor, hence the pressure drop for randomly placed packings.

2.3 Mass transfer in a fluidized bed

A bubbling fluidized bed has an efficient solid-gas mass transfer rate due to the good contact between the phases from proper mixing and having a uniform concentration in the bed. This is important for reaction efficiency and having a homogeneous temperature distribution is thus favorable for CLC. [24]. Two phase theory can explain the solid-gas mass transfer in a fluidized bed. The theory assumes that there is a dense emulsion phase and a bubble phase in the bed. This in turn gives that the bubble flow rate is equal to the excess gas flow above the minimum fluidization. The bubble phase flow rate can be obtained by equation 2.9 [25] where Coefficient Y for Group B particles is in a range of 0.6 to 0.8. [17]

$$G_b = Y(U_g - U_{mf})A \tag{2.9}$$

From theory it can be seen that the mass transfer only occurs between the bubbling and emulsion phases.The mass transfer rate decreases with an increase in bubble size [24]. While small bubbles, due to bubbling fluidization, is desirable for effective mass transfer, large bubbles can have the opposite effect by causing bypassing and slugging [22].

2.4 CLC fuel conversion rate

The fuel conversion rate for CLC can be obtained through the chemical reaction and mass balance equations and the general reduction–oxidation reactions in both reactors are described in equation 2.10 (fuel reactor) and 2.11 (air reactor) [26]. Me_xO_y is the fully oxidized oxygen carrier and Me_xO_{y-1} is the reduced oxygen carrier.

$$FR : C_nH_m + (2n + 0.5m)Me_xO_y \rightarrow nCO_2 + 0.5mH_2O + (2n + 0.5m)Me_xO_{y-1} \tag{2.10}$$

$$AR : Me_xO_{y-1} + 0.5O_2 \rightarrow Me_xO_y \tag{2.11}$$

The specific reaction in a fuel reactor with CO fuel is given in equation 2.12.

$$2CO + O_2 \rightleftharpoons 2CO_2 \tag{2.12}$$

The specific reaction in a fuel reactor with Syngas fuel is given in equation 2.13:

$$CO + H_2 + O_2 \rightleftharpoons CO_2 + H_2O \tag{2.13}$$

Important parameters regarding for the oxygen carrier is the mass based conversion ω of the oxygen carrier is obtained using equation 2.14 [14] and X is a fraction of oxygen mass that can be transferred and mass of fully oxidized oxygen carrier.

$$\omega = \frac{m}{m_{ox}} = 1 - X \tag{2.14}$$

These equations are relevant for the fuel conversion calculations covered in section 3.5.

Fuel conversion is based on the gas yield, Γ, which is a measurement of the ratio of formed product to consumed reactant. [26] In the case of Syngas, the inlet and outlet flows must be accounted for as water is condensed prior to the analysis[13].

$$\Gamma_{syngas} = \frac{Y_{CO_2,out} + Y_{H_2,in} - Y_{H_2,out}}{Y_{CO_2,out} + Y_{CO,out} + Y_{H_2,in}} \tag{2.15}$$

$$\Gamma_{CO} = \frac{Y_{CO_2,out}}{Y_{CO_2,out} + Y_{CO,out}} \tag{2.16}$$

2.5 Water-gas shift reaction

The water-gas shift reaction is a reaction that occurs between carbon monoxide and hydrogen as shown in equation 2.17. It is used in industry and is a weak, temperature dependent, exothermic, reversible reaction that usually requires a catalyst.[27][28]

$$CO + H_2O \rightleftharpoons CO_2 + H_2 \tag{2.17}$$

A precise equilibrium constant is given by equation 2.18.[28]

$$k_{eq} = 10^{\frac{5693.5}{T} + 1.077ln(T) + 5.44*10^{-4}T - 1.125*10^{-7}T^2 - \frac{49170}{T^2} - 13.148} \tag{2.18}$$

but a simplified equation of the constant for the reaction is given by equation 2.19 [28]

$$k_{eq,simplified} = exp(\frac{4577.8}{T} - 4.33) \tag{2.19}$$

The temperature that is to be examined in this project is approximately 840 °C and the equilibrium constant obtained using equation 2.19 is circa 0.8. This implies that the reaction should not favor either side. The reaction has been observed in CLC studies and has shown a possibility of the produced gas composition being affected, resulting in an increased fuel conversion rate.[29]

3
Methods

The main experiments are conducted at the M7 lab at Chalmers and the CLC lab is used for measurements of Ilmenite density.

3.1 Preparation

Before the experiments can be initiated in a reactor, density and the mass of packings, as well as density of the bed material needs to be determined. This allows the calculation of the mass of packings and bed particles, and the reaction time of the experiments.

3.1.1 Void factor and density and mass of packings

The packings used in these experiments are *RMSR 25-3* and *Hiflow® ring 25-5 metal*. Both are made of stainless steel but have different geometries, as can be seen in Figure.3.1 and Figure.3.2.

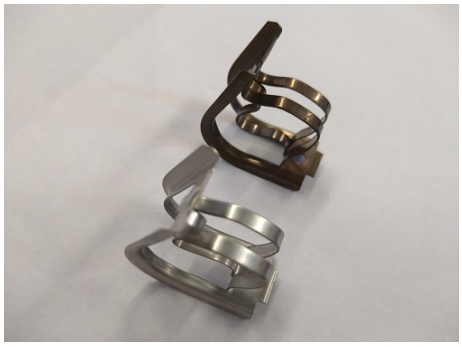

Figure 3.1: RMSR packing

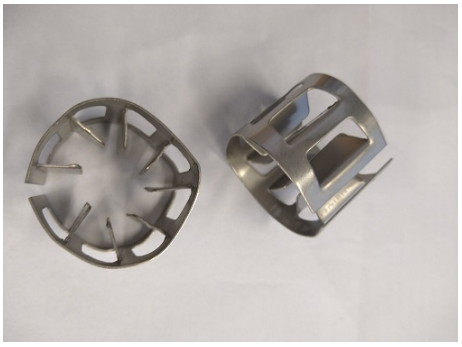

Figure 3.2: Hiflow® ring packing

A void factor ϵ indicates the fraction of space that is not occupied by packings. This needs to be determined for both types of packings when calculating the residence time of the fuel as well as the amount of Ilmenite required to reach the desired bed height. To find the void factor of the packing material, an empty container is completely filled with water and the added water weighed. The weight of liquid is m_{tot}. The container is then emptied and completely filled with packings. Water is then added into the container until it is completely full and weighed. The weight of the newly added water is m_{void}. The void factor is then given by equation 3.1.

$$\epsilon = \frac{m_{void}}{m_{tot}} \tag{3.1}$$

Assuming that the reactor is to be filled with packings up to 1.1 m, to account for bed expansion, the volume of the reactor that needs to be filled with packings is calculated using the cross-sectional area of the reactor, which in this case is 0.0048 m^2. The mass of packings required are calculated by multiplying the volume of the reactor, the void factor, and the density of the packings and shown table 3.3 in section 3.4.2.

3.1.2 Measurement of Ilmenite's density

Ilmenite is chosen for the bed particles as well as the oxygen carrier in this experiment. Ilmenite density is measured for the calculation of reaction time as well as to compare before and after the Syngas experiment. This is to assure that there is no change in Ilmenite quality.

A density apparatus, which can be seen in figure 3.3, is utilized. The cylindrical silver metal container is filled by adding ilmenite through the funnel. When it is filled completely, a metal spatula is used to assure that the surface is smooth at the container height, then the amount of Ilmenite in the container is weighed. This is repeated at least ten times and then the average measured mass is used. All mass measurements are shown in A.1 in Appendix I. The volume of the container is known, in this case is 25.092*10^{-3} m^3, therefore the density can be easily obtained by dividing the measured mass by the volume.

Figure 3.3: Density apparatus

3.1.3 Calculation of reaction time

A total gas velocity of 0.3 m/s is required for sufficient bubbling fluidization, which is described in the theory section. This is equivalent to a flow rate of 21 normal liters per minute (nlpm). As the maximum possible mass flow is 15 nlpm for fuel, the rest is compensated by adding 6 nlpm of nitrogen gas. Assuming that the Ideal

gas law applies, a volume of 1 nm^3, a temperature of 278 K and a pressure of 101.3 kPa, an amount of substance of 44.6 mole per nm^3 is obtained. The molar flow rate in moles per minute, for both fuel and needed oxygen, is calculated by multiplying each flow rate with the amount of substance. The Ilmenite mass is calculated by multiplying the cross-sectional area of the bed, the bed height and the Ilmenite density obtained by the method described in section 3.1.2. If packings are used, the resulting mass is also multiplied with the void factor obtained as described in section 3.1.1. Based on an assumed 0.72 weight percent Ilmenite conversion and the calculated Ilmenite mass, the required oxygen mass can be calculated. Multiplying the amount of substance of oxygen and the oxygen flow rate gives the time needed for the reaction. The calculated reaction time and Ilmenite mass for each tested configuration can be found in table 3.3, section 3.4.2.

3.2 Reactor

A laboratory scale *253 MA* vertical steel reactor, as shown in Fig.3.4, is used for the experiment. The furnace is insulated and has a height of 1.27 m and an inner diameter of 78 mm. There are holes on both the front and back side of the furnace where eight tubes are connected as seen in Fig.3.5. The tubes on the back are connected with thermocouples and pressure sensors and the ones on the front can be connected to a tube which collects gas samples. The difference that needs to be noted is that the tubes on the back connected at an angle of 40 degrees against the furnace. The furnace is heated electrically and the temperature kept at the desired input temperature. A furnace outlet is open but surrounded by a metal fume hood. Therefore it is extremely important to turn on the ventilation when dealing with harmful gases.

Figure 3.4: Outside of the reactor

Figure 3.5: Inside of the reactor

The measurement points are located as in figure 3.7 and the heights are listed in table 3.1. The same height is used for the temperature, pressure measurement and sample collection points. The distributor plate is a plate of 5 mm thickness, with 61 holes of 0.6 mm diameter, where fuel, air and N_2 were introduced. To stop small bed particles from falling into or filling the holes it is important to always have a gas flow. Every other time, when emptying the reactor, the wind box is also opened and checked to assure that the holes are not clogged. A sample of gas is sent to a sensor *SICK* placed right next to the reactor as in Figure.3.6. SICK is originally used for measuring slow changes in gas concentration, but it is possible to obtain the change in smaller units of time, such as seconds. The sensor is connected to a software which shows the composition of gas in volume percent (vol%) for each gas component. It also shows temperature and pressure change and flow rate over time of each gas for both inlet and outlet.

Table 3.1: Height of measurement points for the reactor

Measurement Point	Height [cm]
MP8/TP8	79.65
MP7/TP7	63.65
MP6/TP6	47.65
MP5/TP5	31.65
MP4/TP4	15.65
MP3/TP3	13.65
MP2/TP2	8.88
MP1/TP1	3.65

Figure 3.6: Reactor and sensor SICK

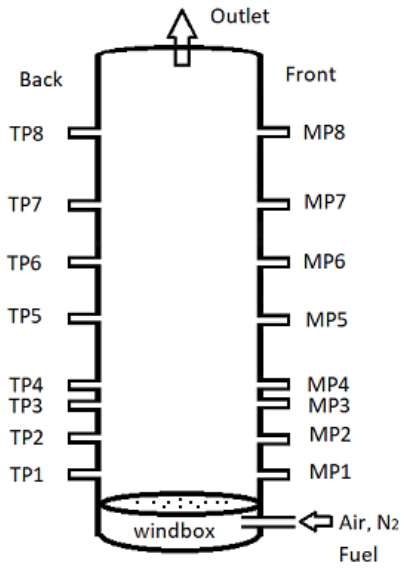

Figure 3.7: Measurement point locations for the setup. Reactor dimension may not be to scale.

3.3 Test and calibration

In order to ensure stable measurements, sensor tests are to be conducted every other experiment day. If the outlet concentration of calibration gases deviates from the inlet, calibration needs to be done. The procedure is as follows:

1. Change the sensor to "calibration" mode, make sure the pump is off and that valves for test gases are open.
2. Flood the calibration sample chamber with N_2 to remove other gases. Do this until O_2 and CO are shown as zero vol% for five minutes.
3. Introduce a gas mixture with NO, SO_2, CO and CO_2 and check if the outlet sensor shows same concentration for CO_2 as the inlet sensor.
4. Repeat the test with 9 vol% of O_2 and confirm that the inlet and outlet sensors agree.
5. Repeat the test with 90 vol% of CO_2 and confirm that the inlet and outlet sensors agree.
6. Finally test with Syngas at 50 vol% CO and 50 vol% H_2 and confirm that the inlet and outlet sensors agree.

If the concentration deviation is larger than 0.1 vol% at any of the steps between three to six, calibration is needed. This can be done automatically through software It should be noted that the sensor is calibrated based on Syngas, so the last step should always be based on Syngas even when test is done before the experiments with CO.

3.4 Experiments

In this section, the detailed procedure for both the empty bed and main experiments are described.

3.4.1 Empty bed experiment

Packings used in the experiments are made of stainless steel, which usually has strong resistance against oxidization. However, as with any object that contains iron, there is still a possibility that stainless steel oxidizes. It is crucial that solely the bed particles act as oxygen carriers for these experiments. Therefore experiments without bed particles are conducted to ensure that the packings themselves are minimally involved and have a negligible effect on the oxidizing process during the experiments. Syngas is studied for possible water-gas shift effect but the measured change depends solely on if packings are affecting the conversion by carrying oxygen, and the fuel itself should not have an effect. Therefore only CO is tested with both packings for this experiment. In addition to an empty reactor with only packings, a completely empty reactor is also tested to eliminate other possible effects such as re-circulation of air or air being left in the reactor. The procedure is as follows:

1. If not testing a completely empty reactor, add packings into the bed while an air flow is sustained
2. Introduce N_2 at a flow of 10 nlpm
3. Introduce CO at a flow of 15 nlpm and inert nitrogen at 6 nlpm for 40 seconds
4. Observe the outlet concentration of CO
5. Repeat steps 2-4 at least two times

The temperature is set to 840 °C and the measurement point is at MP8 for these experiments.

3.4.2 Packed fluidized bed experiment

As mentioned in section 3.1.1, void factors and packing mass are needed when filling the reactor with packings. The results are almost identical to the product data provided by the manufacturer, 0.97 for RMSR and 0.96 for Hiflow® ring.

Table 3.2: Experimentally determined void factor and mass of packings for RMSR and Hiflow® ring

	No packings	RMSR	Hiflow® ring
Void factor [-]	1	0.96	0.95
Packing density [kg/m^3]	-	195	271
Packings mass [kg]	-	0.984	1.356

Furthermore, reaction times for each set of experiments are obtained based on the method in section 3.1.3 and using the calculated void factors. See table 3.3 for the detailed results. As the fuel flow is set to 21 nlpm for both Syngas and CO experiments, the reaction time and Ilmenite mass is the same for equal bed heights.

Table 3.3: Ilmenite mass and reaction time used for the experiments

	Ilmenite mass [g]			Reaction time [s]		
	No packings	RMSR	Hiflow® ring	No packings	RMSR	Hiflow® ring
10 cm	782.09	748.71	742.99	32	30	30
15 cm	1173.14	1123.07	1114.48	48	45	45
20 cm	1564.19	1497.43	1485.98	64	60	60
25 cm	1955.23	1871.79	1857.47	80	75	75
30 cm	2346.28	2246.14	2228.97	96	90	90
35 cm	2737.33	2620.50	2600.46	112	105	105
40 cm	3128.37	2994.86	2971.96	128	120	120
50 cm	3910.47	3743.57	3714.94	160	150	150
55 cm	4301.51	4117.93	4086.44	176	165	165
60 cm	4692.56	4492.29	4457.93	192	180	180

Since the fuel conversion rate is a key factor that needs to be verified at the outlet of the bed, a gas sample is taken at MP8. As the investigated bed has a maximum height of 60 cm, and taking into account the expansion of the bed, MP8 which is located at 79.65 cm from the bottom of the distribution plate is suitable. The temperature of the furnace is set to 840 degrees C, which is in the typical range for combustion in a fluidized bed (800-1000 degrees C)[30].

The experiments start with setting the target temperature of the furnace, adding any desired packings while the air flow rate is set between 15-21 nlpm. When the temperature reached above 840 °C for all measurements points and stabilized, bed particles can be added. The first part of the experiment always starts with adding air flow so that the minimum required oxygen level is reached. This allows the Ilmenite to capture and store oxygen in its pores. The following step is to change the gas flow to nitrogen gas so that excess oxygen is removed from the furnace. Finally fuel gas and nitrogen are introduced for the duration of the calculated reaction time. To clean the reactor and make sure that no fuel or product of the reaction are left after the reaction is completed, the reactor is flooded with nitrogen gas. Exact experimental steps are as follows:

1. With oxygen levels at or above 20 vol% and a air flow of 6 nlpm (in order to avoid bed particles from flowing out from the bed), add bed particles to the reactor.
2. Set the air flow rate back to 21 nlpm and wait until oxygen levels are higher than 20.75 vol% for bed height up to 35 cm, and 20.7 vol% for bed heights above that.
3. When the temperature and pressure have stabilized, set N_2 to 10 nlpm until oxygen is lower than 0.45 vol% for bed heights up to 35 cm, and 0.76 vol% for bed heights above that.
4. Change the N_2 flow rate to 6 nlpm and introduce Syngas or CO at 15 nlpm for the duration of the calculated reaction time.
5. Stop the fuel and set the N_2 flow rate to 10 nlpm.
6. When N_2 has been introduced for 5 minutes and no CO and CO_2 concentration is shown, go back to step 2 and repeat the same procedure two to three more times. For the first experiment run of the day, at least four repetitions are recommended. For new bed heights, go back to step 1.

If spouting of bed particles from the top of the furnace is a risk, especially for higher beds, a metal pipe can be placed over the furnace outlet. To increase the cross-sectional area and decrease the particle velocity thus preventing the bed particles from jumping out of the reactor, a funnel like tube was originally considered. However, the implement seen in figure 3.8 was the only available instrument at the time. Figure 3.9 shows an improved version that can be stably fastened to the reactor using a bolt. Tests confirmed that this did not affect the pressure or temperature.

Figure 3.8: A pipe used for Syngas experiments

Figure 3.9: A pipe used for CO experiments

3.5 Calculation of conversion rates

Both fuel and CO conversion rates, as well as pressure drop, need to be calculated from the obtained data. The total outlet gas flow is the sum of the measured gas flows of nitrogen and fuel during the reaction. Assuming the ideal gas law applies, the total molar flow rate $\dot{n}_{tot}$ at the outlet can be calculated using equation 3.2.

$$\dot{n}_{tot} = \frac{qP}{RT} \tag{3.2}$$

In the above, q is the total flow rate in normal liters per minute, which is obtained from the experiments. P is atmospheric pressure, R is the gas constant and T is the temperature in Kelvin.

Since the volume percentage concentration of each gas species x_i is measured during the experiments, the molar flow rate $\dot{n}$ for each gas, H_2, CO_2 and CO, can be obtained. Based on equation 2.15 and what was mentioned in section 2.4, the fuel conversion rate calculation for Syngas requires that H_2 must be accounted for at the inlet and outlet. This leads to the total conversion based on the lower heating value which is derived as follows[13]:

$$\gamma_{syngas} = 1 - \frac{\Delta H_{H_2}\dot{n}_{H_2,out} + \Delta H_{CO}\dot{n}_{CO,out}}{\Delta H_2\dot{n}_{H_2,in} + \Delta H_{CO}(\dot{n}_{CO,out} + \dot{n}_{CO_2,out})} \tag{3.3}$$

The lower heating value ΔH for H_2 and CO/CO_2 are 244 J/mol and 283.24 J/mol respectively. [31] Calculating the fuel conversion rate for CO and the CO conversion

rate of Syngas is done using equation 3.4[13]. The conversion rate of H_2 is calculated using equation 3.5[13].

$$\gamma_{CO} = 1 - \frac{\dot{n}_{CO,out}}{\dot{n}_{CO,out} + \dot{n}_{CO_2,out}} \tag{3.4}$$

$$\gamma_{H_2} = 1 - \frac{\dot{n}_{H_2,out}}{\dot{n}_{H_2,in}} \tag{3.5}$$

The mass conversion rate ω of the oxygen carrier changes over time. It cannot be measured directly and needs to be calculated from the measurement data. ω for each time step is obtained from equation 3.6 for Syngas and equation 3.7 for CO, both which are based on the oxygen conversion rate, which in turn is obtained from equation 2.14

$$\omega_t = \omega_{t-1} - \int_{t-1}^{t} \frac{\dot{n} M_O}{m_{ox}} (2x_{CO_2} + x_{CO} - x_{H_2}) \tag{3.6}$$

$$\omega_t = \omega_{t-1} - \int_{t-1}^{t} \frac{\dot{n} M_O}{m_{ox}} (x_{CO_2}) \tag{3.7}$$

where M_o is the molar mass of oxygen and x is the composition of each gas species.

The fuel conversion is calculated with an oxygen conversion span between 0.992 and 0.999. This is to avoid extreme changes in conversion rate when the fuel is introduced, at which point the rate is assumed to be $0.999 < \omega < 1$, and to avoid low conversion rate when $\omega < 0.992$ and the conversion rate starts to drop. The conversion rate is calculated as the average rate during this interval. Most of the tests are repeated at least three times per setup. For the first setup after emptying the reactor, at least four measurements are taken and of those the last three are used.

The pressure drop of the bed can be calculated from the atmospheric pressure, the pressure in the wind box and the pressure over distributor plate. But it is assumed that P_{atm} is the reference pressure and thus zero.

$$\Delta P_{bed} = -P_{atm} - _{dp} + P_{WB} = -\Delta P_{dp} + P_{WB} \tag{3.8}$$

Pressure drop for each bed height is calculated using equation 3.8, where pressure at windbox P_{WB} is obtained from measured data and pressure over distributor plate ΔP_{DP} is obtained from an empty experiment set up, without packings or bed particles in the reactor and only an air flow rate of 15 nlpm. The pressure drop between MP1 and the windbox should be equivalent to the pressure drop over the distributor plate.

4
Results

In this chapter, the results are presented. This includes fuel conversion rates, temperature and pressure change over time, pressure drop of the bed and density analysis of Ilmenite.

4.1 Fuel conversion

Table 4.1 shows the average calculated total fuel conversion rates for both Syngas and CO, with different bed heights, as well as with different packings, including no packings. The results are also plotted and shown in figure 4.1 and 4.2.

Table 4.1: Average fuel conversion rates for CO and Syngas fuels, with bed heights from 10 to 60 cm, using RMSR, Hiflow® ring or no packings

	Syngas			CO		
	No packings	RMSR	Hiflow® ring	No packings	RMSR	Hiflow® ring
10 cm	0.6897	0.8425	0.7768	0.6140	0.7864	0.6662
15 cm	0.7125	0.8813	0.8127	0.6412	0.8057	0.7504
20 cm	0.8551	0.9320	0.8769	0.7027	0.9271	0.7048
25 cm	0.8802	0.9610	0.9210	0.8232	0.9544	0.7703
30 cm	0.9188	0.9531	0.9283	0.8286	0.9812	0.9164
35 cm	0.9540	0.9760	0.9832	0.7882	0.9838	0.9460
40 cm	0.9839	0.9927	0.9868	0.8688	0.9923	0.9840
50 cm	0.9639	0.9955	0.9961	0.9639	0.9980	0.9922
55 cm	0.9694	0.9988	0.9977	0.9651	0.9995	0.9994
60 cm	0.9824	0.9985	0.9978	0.9675	0.9991	0.9993

Table 4.2 shows the average calculated CO conversion rates for Syngas, with different bed heights, as well as different packings, including no packings.

Table 4.2: Average CO conversion rates for Syngas fuels, with bed heights from 10 to 60 cm, using RMSR, Hiflow® ring or no packings

	No packings	RMSR	Hiflow® ring
10 cm	0.6199	0.8382	0.7733
15 cm	0.7003	0.8792	0.7940
20 cm	0.8511	0.9316	0.8712
25 cm	0.8748	0.9616	0.9169
30 cm	0.9173	0.9475	0.9207
35 cm	0.9533	0.9742	0.9832
40 cm	0.9796	0.9929	0.9866
50 cm	0.9621	0.9953	0.9965
55 cm	0.9687	0.9987	0.9980
60 cm	0.9823	0.9986	0.9979

Both table 4.1 and 4.2 show that the conversion rate increases with increasing bed heights. In general the highest rates are achieved during experiments using RMSR packings in combination with either fuel type. Hiflow® ring packings do perform better in some cases but even then the performance is close.

Table 4.3 shows the average calculated conversion rates of hydrogen gas for Syngas fuel, with different bed heights, as well as different packings, including no packings.

Table 4.3: Average H_2 conversion rates for Syngas fuels, with bed heights from 10 to 60 cm, using RMSR, Hiflow® ring or no packings

	No packings	RMSR	Hiflow® ring
10 cm	0.6723	0.9666	0.8847
15 cm	0.9386	0.9649	0.9698
20 cm	0.9774	0.9503	0.9849
25 cm	0.9579	0.9537	0.9750
30 cm	0.9817	0.9923	0.9875
35 cm	0.9767	0.9929	0.9897
40 cm	0.9807	0.9904	0.9916
50 cm	0.9907	0.9983	0.9888
55 cm	0.9928	1.0000	0.9922
60 cm	0.9913	0.9937	0.9977

Resulting fuel conversion rates, using RMSR, Hiflow® ring or no packings, are plotted against different bed heights in figure 4.1 for Syngas fuel and figure 4.2 for CO fuel. The conversion rates are calculated by the measured data at a temperature of 840 °C and the measurement point MP8. CO conversion rates for Syngas experiments are plotted in figure 4.3. The trendlines shown in the figures are obtained using the polynomial function provided by Microsoft Excel 365. It only shows the general trend of the data points and therefore should not be considered an accurate model.

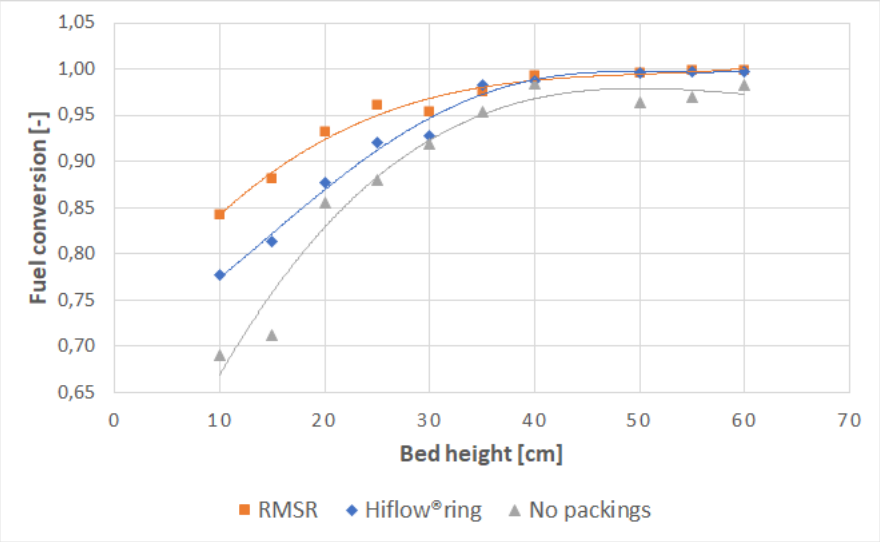

Figure 4.1: Fuel conversion rate for Syngas fuel at 15 nlpm, N_2 at 6 nlpm, bed heights in the range of 10 to 60 cm, using RMSR, Hiflow® ring or no packings at a temperature of 840°C.

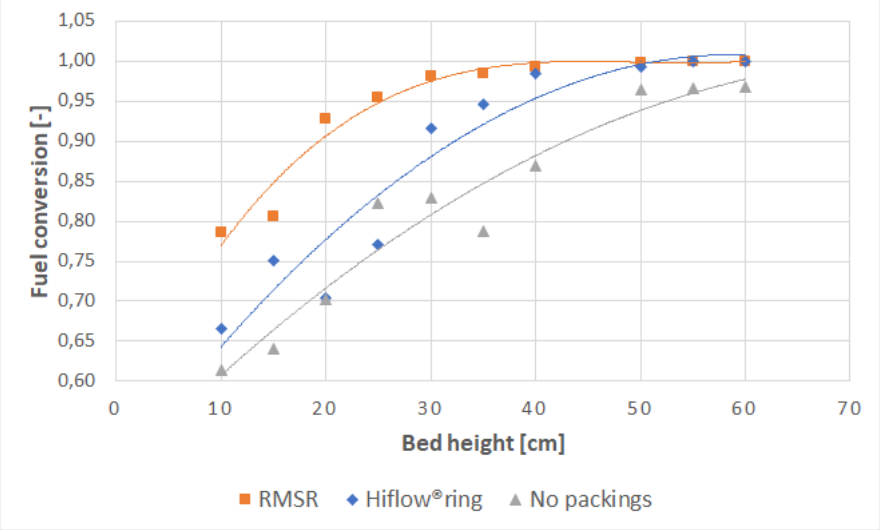

Figure 4.2: Fuel conversion rate for CO fuel at 15 nlpm, N_2 at 6 nlpm, bed heights in the range of 10 to 60 cm, using RMSR, Hiflow® ring or no packings at a temperature of 840°C.

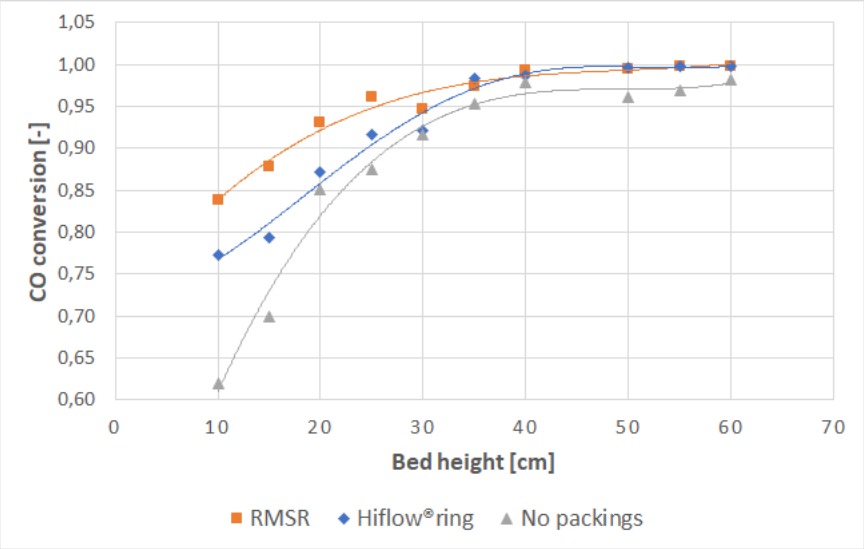

Figure 4.3: CO conversion rate for Syngas fuel at 15 nlpm, N_2 at 6 nlpm, bed heights in the range of 10 to 60 cm, using RMSR, Hiflow® ring or no packings at a temperature of 840°C.

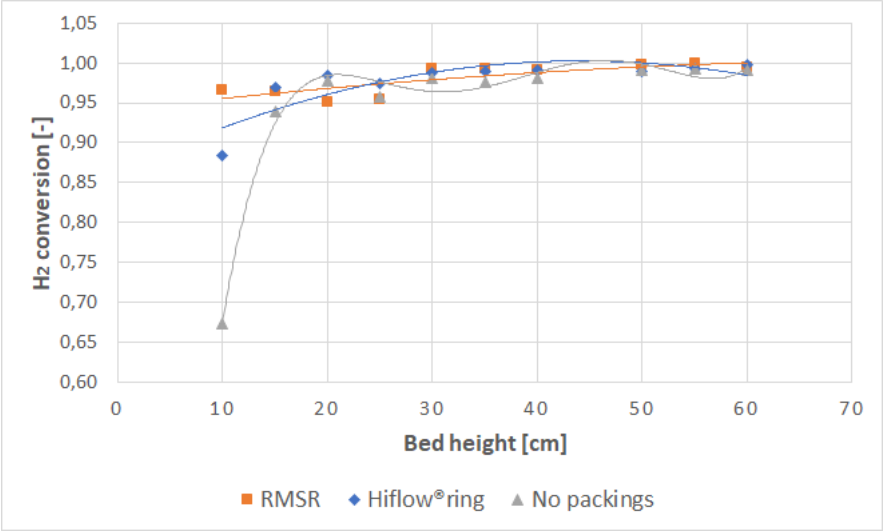

Figure 4.4: H2 conversion rate for Syngas fuel at 15 nlpm, N_2 at 6 nlpm, bed heights in the range of 10 to 60 cm, using RMSR, Hiflow® ring or no packings at a temperature of 840°C.

Figures 4.5 and 4.6 show the actual improvement, when using packings, compared to the theoretical maximum improvement possible for each bed height. The logarithmic function provided by Microsoft Excel 365 is used to obtain the general trend lines.

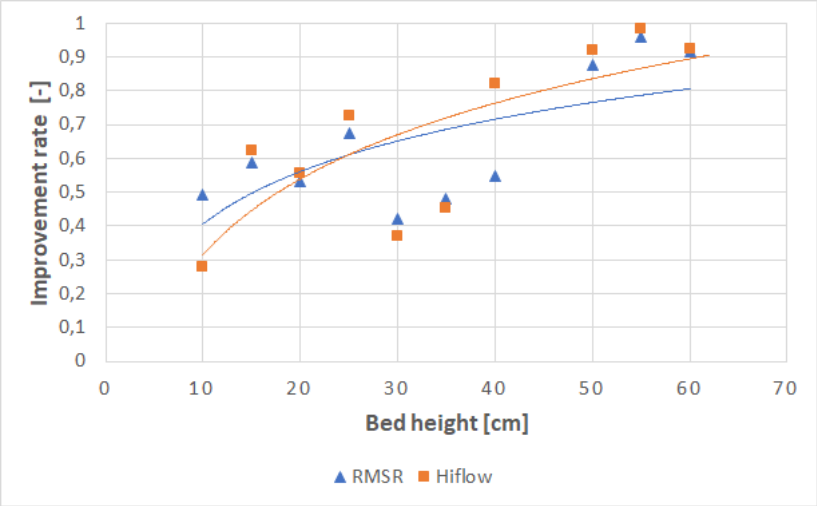

Figure 4.5: Syngas fuel conversion rate improvement when using packings in comparison to the theoretical maximum.

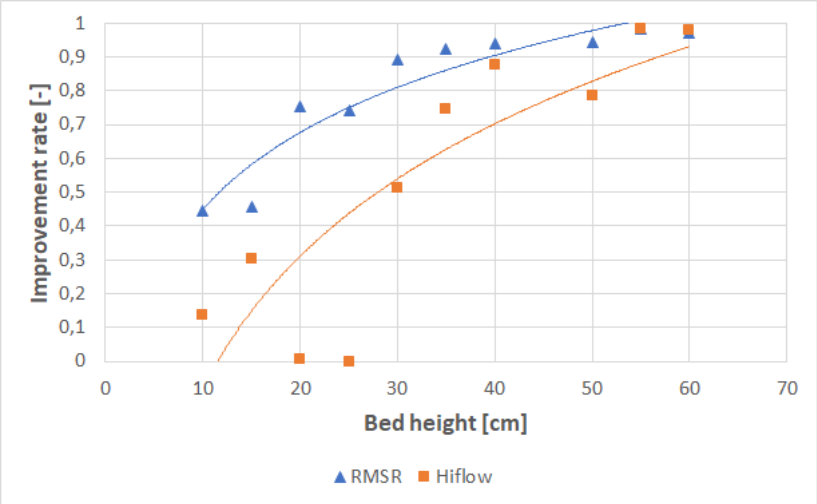

Figure 4.6: CO fuel conversion rate improvement when using packings in comparison to the theoretical maximum.

In figure 4.1 and 4.2 the trend similarity of fuel conversion rates in relation to bed height for both Syngas and CO fuels can be seen. For bed heights between 10 and 30 cm, the fuel conversion rates with RMSR is more than 10 % higher than experiments using Hiflow® ring packings and more than 20% higher than without packings. However, the fuel conversion rate is very similar for both packing types when the bed height reaches or exceeds 40 cm. At those heights nearly 100% conversion is

acheived. For all tested bed heights, fuel conversion rates remained lower without packings than with.

The CO conversion rates for Syngas experiments that can be seen in figure 4.3 also share a similar trend to the fuel conversion rates. Experiments with RMSR and a bed height of 10 cm show around a 30 % higher conversion rate compared to the same bed height without packings. The presence of packings provide for higher conversion rates at all tested bed heights but the absolute improvement becomes smaller as the rate approaches 100 %. However when the improvement rate in relation to the theoretical maximum improvement is calculated, it is higher for the higher bed heights, as is shown in figures 4.5 and 4.6. Figure 4.4 shows the conversion rate of H_2. For most bed heights, the conversion rates are above 95 % and production of H_2 cannot be seen. H_2 conversion rates also follow a pattern of higher conversion rates with higher bed heights and/or when using packings.

The fuel and CO conversion rates against Ilmenite mass are plotted in figures 4.7-4.9 and against pressure drop are shown in figures 4.10-4.12. Pressure drops are calculated and shown in table 4.4.

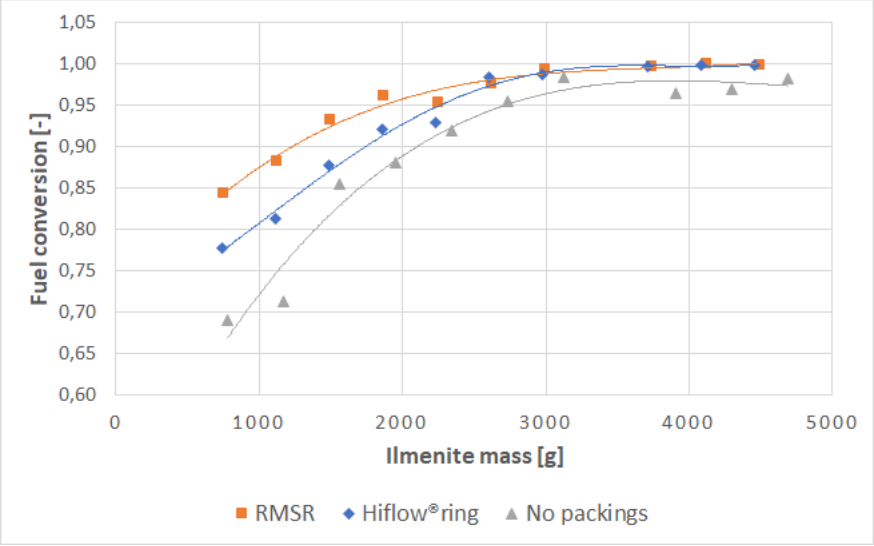

Figure 4.7: Fuel conversion rate for Syngas fuel at 15 nlpm, N_2 at 6 nlpm, against Ilmenite mass, using RMSR, Hiflow® ring or no packings at a temperature of 840°C.

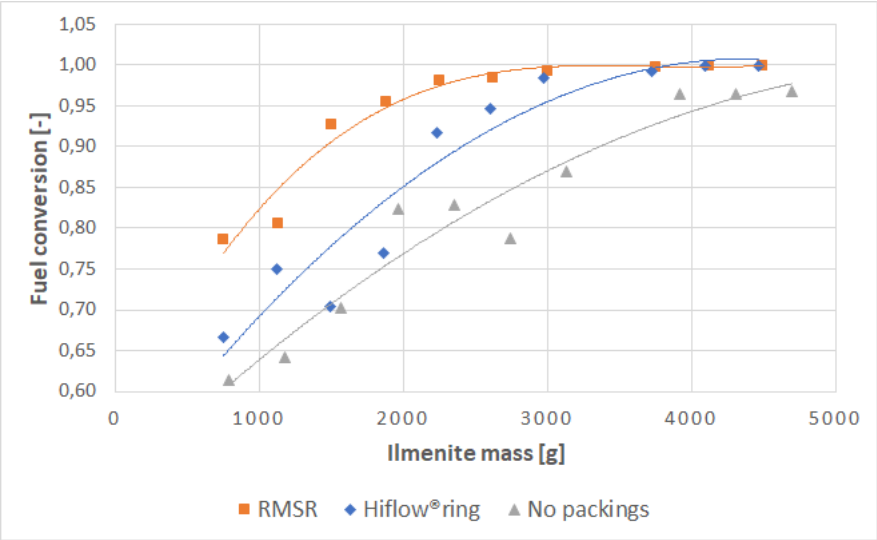

Figure 4.8: Fuel conversion rate for CO fuel at 15 nlpm, N_2 at 6 nlpm, against Ilmenite mass, using RMSR, Hiflow® ring or no packings at a temperature of 840°C.

When fuel conversion rates for both fuels are compared against Ilmenite mass, a similar trend as with bed heights can be seen. The conversion rates increase with the Ilmenite mass, packings improve the conversion rate and experiments using RMSR show the highest rates.

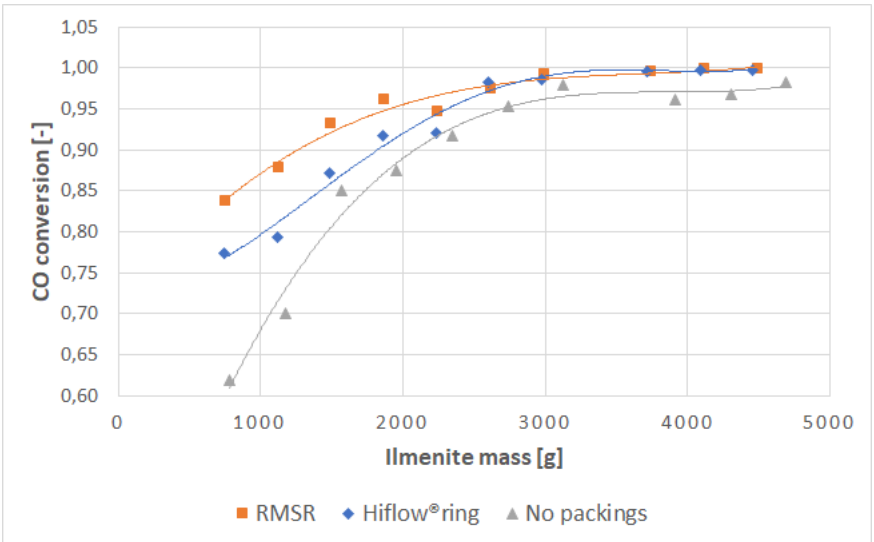

Figure 4.9: CO conversion rate for Syngas fuel at 15 nlpm, N_2 at 6 nlpm, against Ilmenite mass, using RMSR, Hiflow® ring or no packings at a temperature of 840°C.

When CO conversion rates are compared against Ilmenite mass, they once again follow the same pattern as the conversion rates compared against bed heights. At lower Ilmenite mass, the improvement of fuel conversion rates are high, around 20 % higher with Hiflow® ring packings and 30 % higher with RMSR.

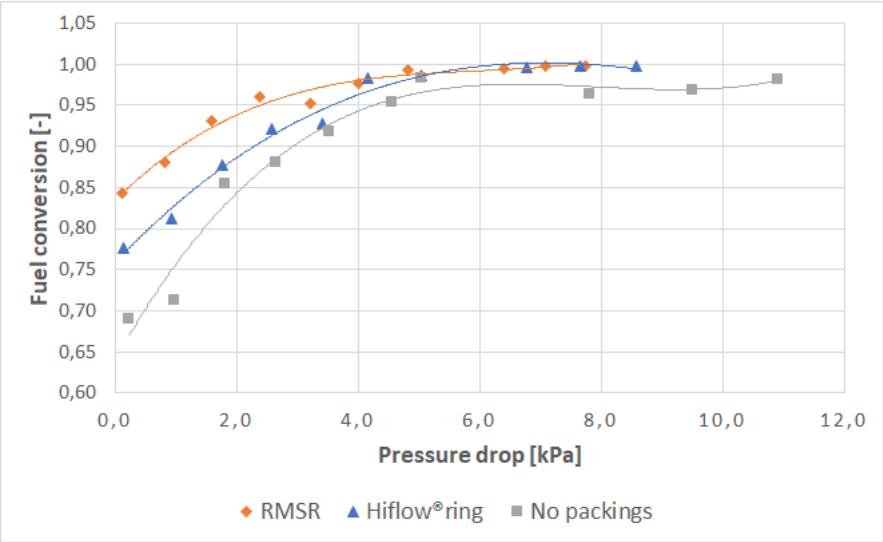

Figure 4.10: Fuel conversion rate for Syngas fuel at 15 nlpm, N_2 at 6 nlpm, against pressure drop, using RMSR, Hiflow® ring or no packings at a temperature of 840°C.

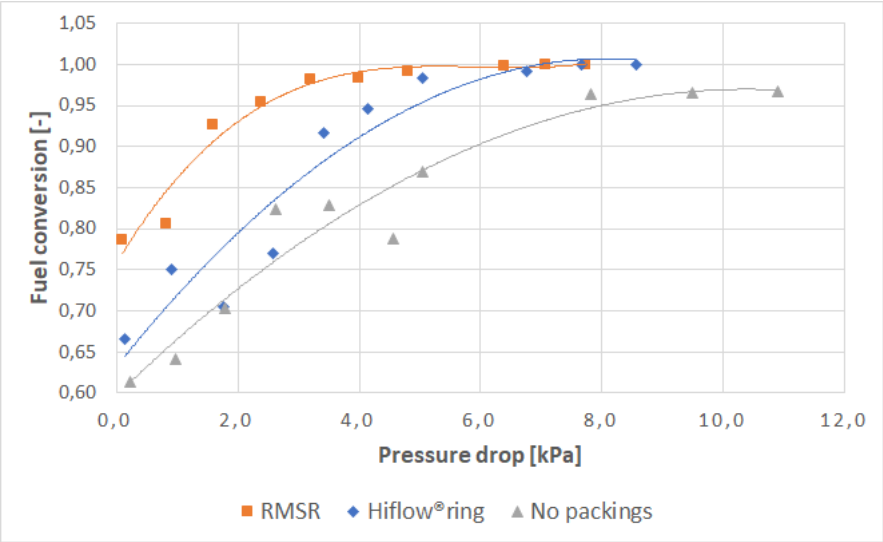

Figure 4.11: Fuel conversion rate for CO fuel at 15 nlpm, N_2 at 6 nlpm, against pressure drop, using RMSR, Hiflow® ring or no packings at a temperature of 840°C.

When the conversion rates are plotted in terms of pressure drop, as can be seen in figure 4.10 and 4.11, an improvement of the fuel conversion rates can be seen when packings are used.

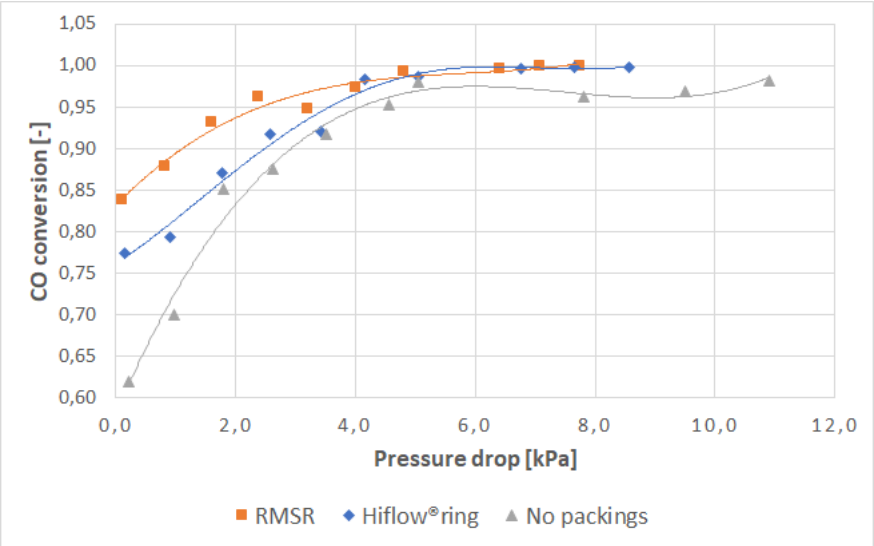

Figure 4.12: CO conversion rate for Syngas fuel at 15 nlpm, N_2 at 6 nlpm, against pressure drop, using RMSR, Hiflow® ring or no packings at a temperature of 840°C.

The CO fuel conversion rates during the reaction process, for bed heights of 10, 20, 30, 40, 50 and 60 cm, are plotted against the oxygen carrier conversion rate X. Note that the y-axis is different for each plot. A conversion rate interval of X between 0.001 to 0.01 is used when plotting the figures. For all tested heights and for experiments using Syngas fuel,refer to A.2.

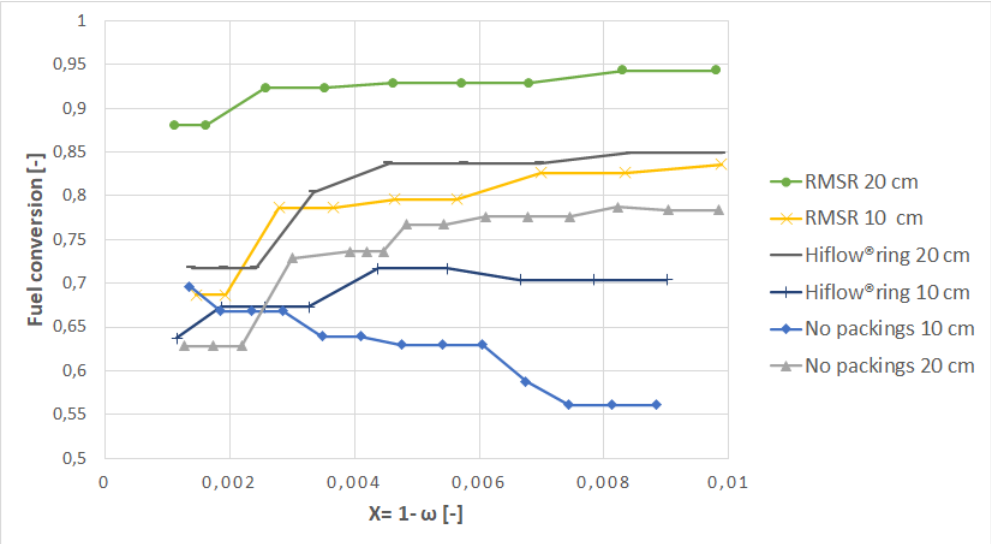

Figure 4.13: Fuel conversion rate versus Ilmenite oxygen conversion rate, using CO fuel, bed heights of 10 and 20 cm, and RMSR, Hiflow® ring or no packings, at 840°C, flow rate of 15 nlpm and 6 nlpm for fuel and N_2 resp.

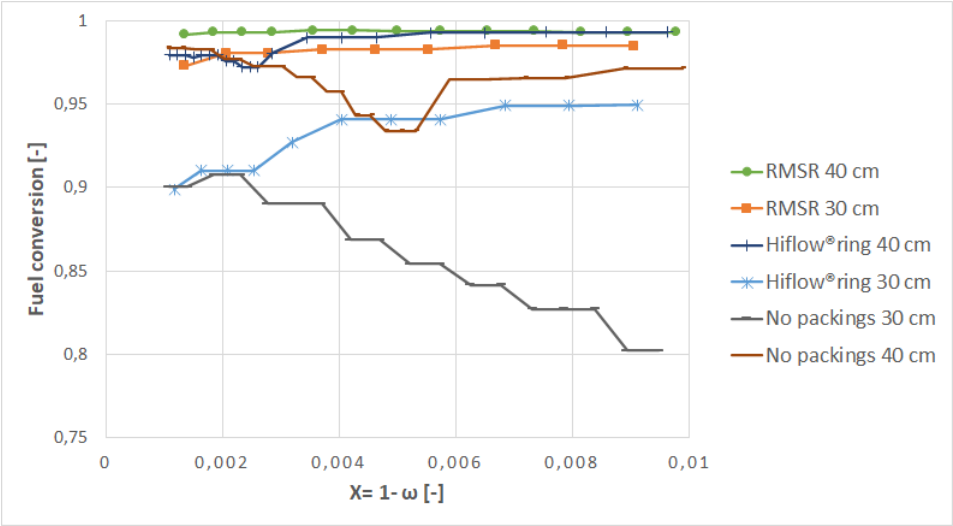

Figure 4.14: Fuel conversion rate versus Ilmenite oxygen conversion rate, using CO fuel, bed heights of 30 and 40 cm, and RMSR, Hiflow® ring or no packings at 840°C, flow rate of 15 nlpm and 6 nlpm for fuel and N_2 resp.

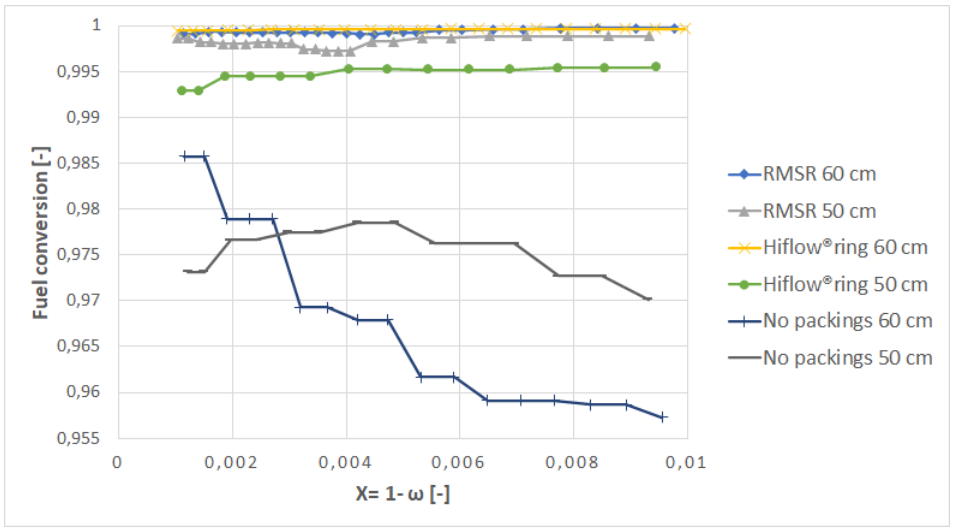

Figure 4.15: Fuel conversion rate versus Ilmenite oxygen conversion rate, using CO fuel, bed heights of 50 and 60 cm, and RMSR, Hiflow® ring or no packings at 840°C, flow rate of 15 nlpm and 6 nlpm for fuel and N_2 resp.

In general, figures 4.13 - 4.15 show an increased stability of the fuel conversion over Ilmenite oxygen conversion as the bed height increases. Packings seem to add extra stability and both RMSR and Hiflow® ring packings result in over 99% fuel conversion rates at bed heights of 50 and 60 cm.

4.2 Temperature

Temperatures during one experiment cycle at the measurement point TP1, with bed heights of 10, 20, 30, 40, 50 and 60 cm and RMSR, Hiflow® ring or no packings, are compared in figures 4.16-4.21. The complete temperature measurement data for all tested heights, including experiments using CO fuel, can be found in A.3 in Appendix I.

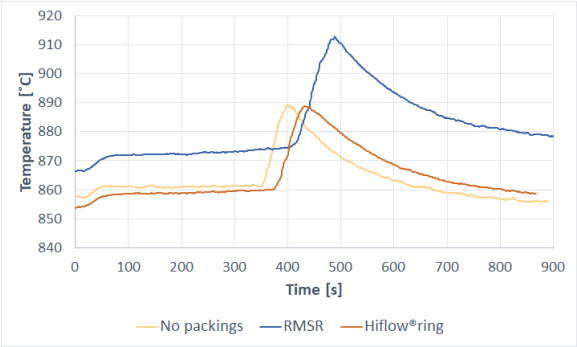

Figure 4.16: Temperature change over time using Syngas fuel, 10 cm bed height and RMSR, Hiflow® ring or no packings.

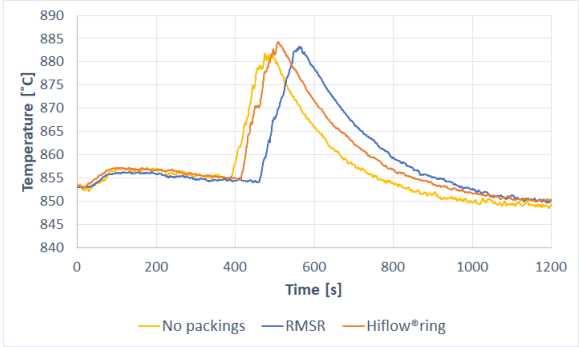

Figure 4.17: Temperature change over time using Syngas fuel, 20 cm bed height and RMSR, Hiflow® ring or no packings.

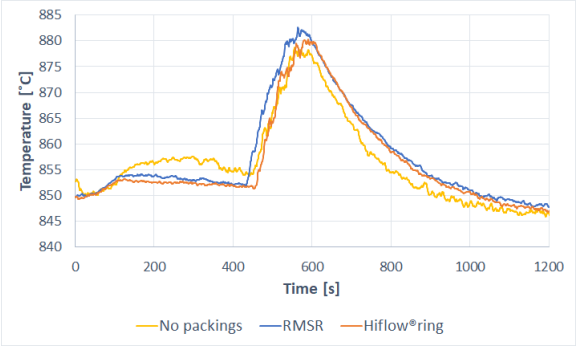

Figure 4.18: Temperature change over time using Syngas fuel, 30 cm bed height and RMSR, Hiflow® ring or no packings.

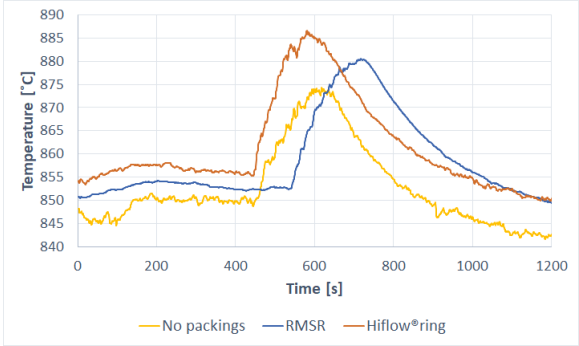

Figure 4.19: Temperature change over time using Syngas fuel, 40 cm bed height and RMSR, Hiflow® ring or no packings.

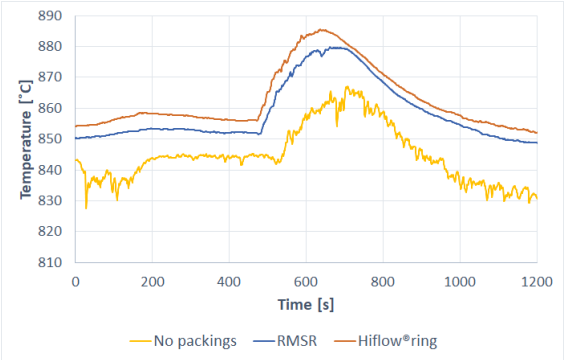

Figure 4.20: Temperature change over time using Syngas fuel, 50 cm bed height and RMSR, Hiflow® ring or no packings.

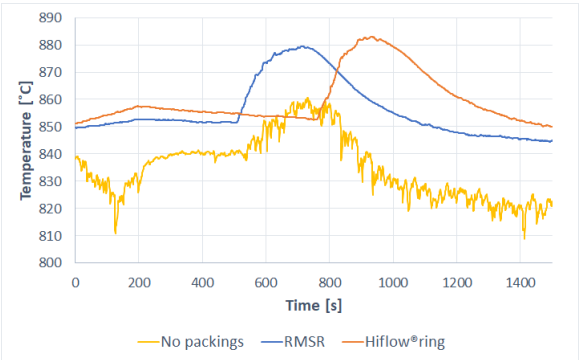

Figure 4.21: Temperature change over time using Syngas fuel, 60 cm bed height and RMSR, Hiflow® ring or no packings.

Temperature change due to the exothermic reaction is consistent in its pattern regardless of bed height or packing type. The temperature increases around 20 to 30 °C during the reaction and returns to the initial temperature. For experiments with higher beds without packings, a significant increase in temperature fluctuations are observed. In figure 4.21 the temperature change over time is shown for different packing types at a bed height of 60 cm. Tests with RMSR and Hiflow® ring packings show a smooth temperature change, while the tests without packings show larger fluctuations. Note that while the targeted temperature is 840 °C for all measurements, the temperature at the measurement points can be slightly different depending on the set up.

4.3 Pressure

Pressure measured at point TP1 over one experiment cycle, with bed heights of 10, 30 and 40 cm, are shown in figures 4.22-4.24. All pressure data for the experiments can be found in A.4 in Appendix I.

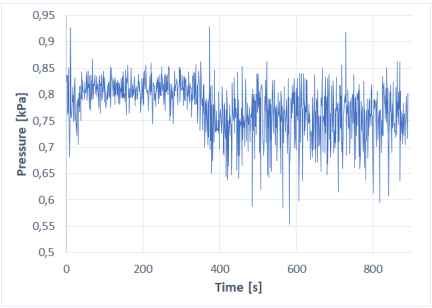

(a) No packings

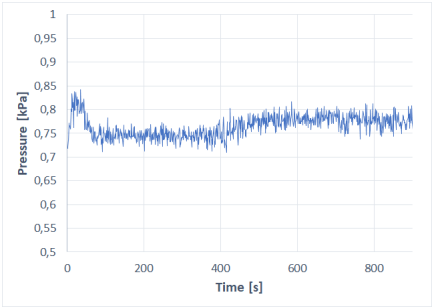

(b) RMSR

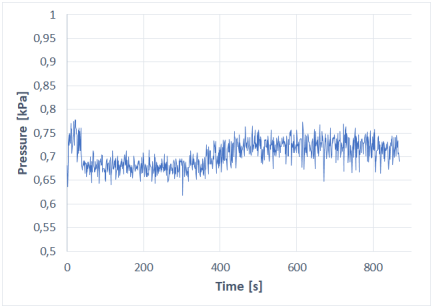

(c) Hiflow® ring

Figure 4.22: Pressure comparison for 10 cm bed height, Syngas fuel and using RMSR, Hiflow® ring or no packings

The pressure measurements clearly show that the experiments without packings have a higher peak amplitude and variation of pressure compared to experiments using packings. RMSR provides the most stable pressure over time, as seen in figure 4.22. This pattern is similar for the pressure measurements up to a bed height of 40 cm, however no prominent variations are observed for bed heights of 50 and 60 cm. This indicates that the pressure reaches its peak value at or around a bed height of 50 cm for MP 1. Therefore the measurements above this height could not be properly obtained.

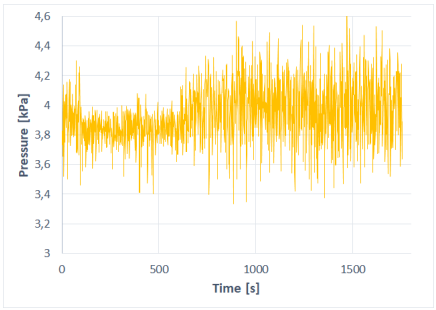

(a) No packings

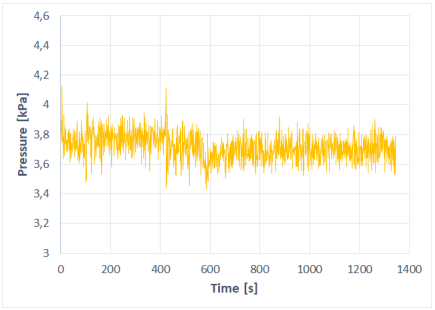

(b) RMSR

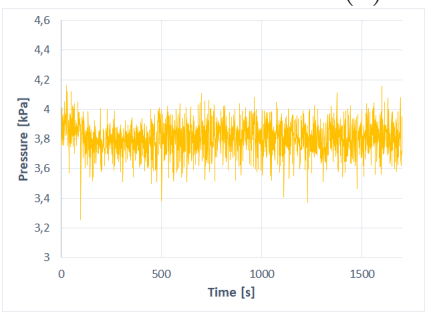

(c) Hiflow® ring

Figure 4.23: Pressure comparison for 30 cm bed height, Syngas fuel and using RMSR, Hiflow® ring or no packings

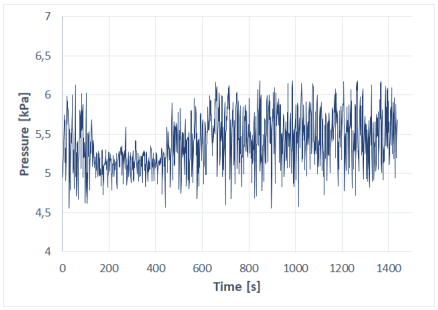

(a) No packings

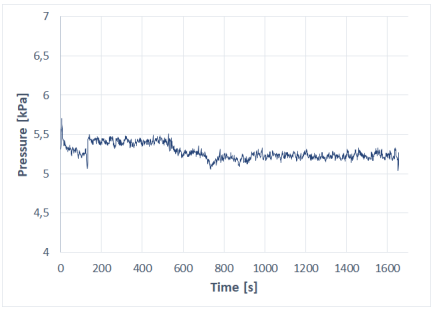

(b) RMSR

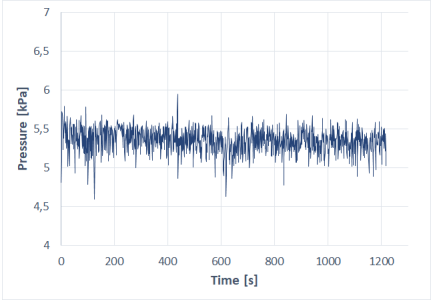

(c) Hiflow® ring

Figure 4.24: Pressure comparison for 40 cm bed height, Syngas fuel and using RMSR, Hiflow® ring or no packings

4.4 Pressure drop

The pressure drop in the bed is calculated using equation 3.8 and the results are presented in table 4.4. The mean pressure is calculated for one experiment cycle.

Table 4.4: Pressure drop [kPa] in the bed for bed heights of 10 to 60 cm, using RMSR, Hiflow® ring or no packings.

	No packings	RMSR	Hiflow® ring
10 cm	0.220	0.104	0.137
15 cm	0.969	0.821	0.914
20 cm	1.793	1.588	1.766
25 cm	2.628	2.378	2.579
30 cm	3.512	3.208	3.413
35 cm	4.553	3.998	4.148
40 cm	5.036	4.809	5.036
50 cm	7.807	6.395	6.769
55 cm	9.492	7.077	7.651
60 cm	10.901	7.734	8.562

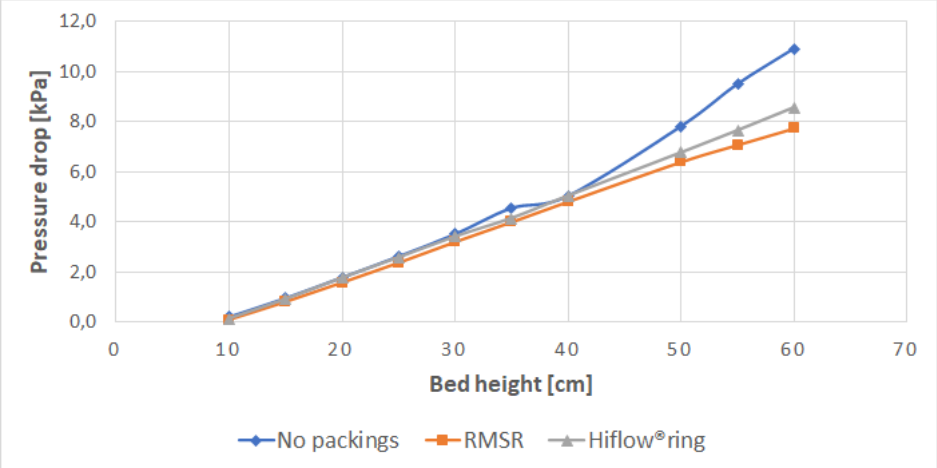

Figure 4.25: Pressure drop against bed heights between 10 to 60 cm using RMSR, Hiflow® and no packings at 840°C, flow rate of 15 lpm and 6 lpm for Fuel and N_2 resp.

When equal bed heights from 10 cm to 40 cm are compared, the pressure drop increases with increasing bed height, from nearly 0 kPa to around 5 kPa. This applies to all experiments using RMSR, Hiflow® ring or no packings. When looking at higher bed heights, the pressure drop without packings increases more than twice as fast as with RMSR or Hiflow® ring packings. The highest pressure drop, 10.9 kPa, is observed during the experiments without packings and a bed height of 60 cm.

4.5 Other observations

During the experiments, a small amount of entrainment was observed but discarded as insignificant. Spouting or large spillage was observed for both Syngas and CO fuels when conducting experiments without packings at a bed height of 50 cm. For the CO experiment, the spilled amount of bed particles was roughly estimated and replaced before continuing the experiment and this might account for some of the observed, sudden pressure change. For the Syngas experiment, the experiment was stopped and completely redone. No other spillages were observed below or above 50 cm of bed height and no spillage occurred during the rerun of the 50 cm bed height experiment with Syngas.

4.6 Density of Ilmenite

Table 4.5: Density of Ilmenite before and after experiments with Syngas

	Before experiment	After syngas experiment
Density[g/m^3]	1637.57	1641.16

The resulting difference for the Ilmenite density calculations before and after the Syngas experiments is less than a 0.2%. The experimentally obtained mass used for the calculations can be found in A.1 in Appendix I.

4.7 Empty bed experiment

In order to ensure the bed particles are the only oxygen carrier during the reaction, empty bed experiments are conduced. Results for the experiments with CO, for each set up, are shown in table 4.6. The average and maximum volume percent CO_2 and CO values at measurement point M8, from the time of fuel injection to when the CO_2 concentration goes back to zero, as well as the calculated oxygen consumption can also be found there.

Table 4.6: Calculated oxygen consumption and average and maximum concentrations of CO and CO_2 for empty bed experiments using CO fuel

	Max CO_2 [vol%]	Avg CO_2 [vol%]	Avg CO [vol%]	Consumed O_2 [g]
No packings	16.20	2.54	10.48	0.34
RMSR	10.57	1.02	5.28	0.28
Hiflow® ring	10.31	1.52	6.99	0.30

The maximum and average CO_2 concentrations are similar for the experiments using RMSR, Hiflow® ring or no packings. The calculated amount of oxygen consumed at most differs by 10% and the amount itself is less than 10 % of the total oxygen used during the experiments. When comparing the experiments using RMSR, Hiflow®

ring or no packings, the empty bed experiment without packings has the highest CO_2 formation and O_2 consumption. In addition to the data in table 4.6, experiments with longer reaction times (300 seconds) were conducted for one Hiflow® ring packings and one no packing configuration. The total O_2 consumption increased to 1.1 g with the Hiflow® ring packings and 1.04 g for no packings. Even an experiment with Sand using RMSR, at the same measurement height, with a reaction time of 40 seconds, resulted in an O_2 consumption of 0.37 g.

5
Discussion

In this section, some interpretations of the results are presented. Possible causes of error and limitations during the experiments, as well as recommendations for further studies, are discussed.

5.1 The effects of different bed heights

Packings increased the fuel conversion rate for all tested bed heights and amounts of Ilmenite. Table 4.1 contains the fuel conversion rates for experiments with Syngas and CO fuel, using RMSR, Hiflow® ring and no packings, and bed heights from 10 to 60 cm. A general trend seems to be that the fuel conversion rate increases with increasing bed height. For 60 cm bed height with RMSR or Hiflow® ring packings, the conversion rate is approaching 100%. This result is repeated in the CO conversion rate for Syngas experiments. As can be seen in figures 4.7 and 4.8, the conversion rate also increases with Ilmenite mass but, the same mass of Ilmenite will also have a higher conversion rate when combined with RMSR or Hiflow® ring packings compared to no packings. The added amount of reactable oxygen and the reaction time is calculated to be equivalent per unit of Ilmenite mass for all bed heights, therefore a difference in oxygen carrier mass should not be behind the observed behavior. At lower bed heights, effects from large bubbles or slugging are unlikely to be a factor as these do not have sufficient time and height for such bubbles to coalesce. It is possible that the effects of fluidization are smaller for lower bed heights compared higher ones, and that part of the observed change in reaction efficiency stems from this. When the reaction path is too short from the distributor plate, it is possible that spouting occurs, causing decreases in fuel conversion rate as the bed height shrinks. This can be supported by the figures 4.13-4.15 where the fuel conversion rate against the conversion rate of oxygen for Ilmenite is stable with higher beds but decreases over time with lower heights. Another possibility is that the theoretically calculated reaction time is not accurate and therefore does not give enough residence time for lower beds. Regardless of these effects, since both a constant amount of oxygen carrier or a constant bed height lead to an increased fuel conversion rate when combined with packings, it can be concluded that packings do provide benefit when that is the goal.

Temperature change over time can be seen in figures 4.16 - 4.21. The temperature fluctuation in terms of amplitude and variance increases with the bed height, which indicates an uneven temperature distribution with the higher beds. Formation of

larger bubbles, slugging or by-passing are possible explanations, however, it is impossible to draw a definitive conclusion from the collected data. This fluctuation is in opposition to the quick and well mixing advantage of a fluidized bed and is an indication of unfavorable conditions when the reaction takes place.

5.2 Comparison between RMSR, Hiflow® ring and no packings

When the results from experiments using RMSR, Hiflow® ring or no packings are compared, the RMSR has the highest overall fuel conversion rates regardless of bed height or fuel type. The fuel conversion rates is in relation to bed height, Ilmenite mass or pressure drop can be seen in figures 4.1 and 4.2, 4.7 and 4.8, and 4.10 and 4.11. Comparing the results with and without packings, the fuel conversion rate is consistently higher when they are present, a result that is in agreement with earlier studies. When compared to higher bed heights, it appears that lower beds have a larger improvement in fuel conversion rates when packings are used. However, since the rate is 96% for the higher beds even without packings, the room for improvement is more limited. When the improvements from packings are compared to the theoretical maximum improvement possible for each bed height, the improvements instead seem to be larger for taller beds. Increasing the conversion rate from 98% to 99.5%, reducing inefficiency by 75%, might be more significant than increasing it from 70% to 85%, a 50% inefficiency reduction.

A previous study suggests that the increases might be due to an improvement of the mass transfer rate through the inhibition of large bubble formation. In accordance with section 2.3, the size of bubbles affects the mass transfer rates and hence the reaction. During two experiment cycles, as described in section 4.5, large spillages occurred. They happened with a bed height of 50 cm, no packings and with both types of fuel, and are assumed to have been caused by slugging pushing bed particles out of the reactor. As mentioned in section 2.1, the large bubble formation occurs thorough the coalescing of small bubbles. This requires a minimum length of path, in this case bed height, which could explain why it was observed at a higher bed height. However, it is unknown why it occurred at 50 cm but not with higher beds, or why repeats of the same experiments did not lead to the same outcome.

When comparing figures 4.22 - 4.24, there exists a variation in pressure change over time for the experiments without packings. Even figures 4.16 - 4.21 show that temperature fluctuations are higher for the case without packings, especially at increasing bed heights. This indicates ineffective fluidization, possibly caused by slugging or large bubbles.

The difference between RMSR and Hiflow® ring packings solely comes from their geometries. Test results point to RMSR having a more suitable geometry for bubble eliminations in general. RMSR has an asymmetric shape that possibly creates a

tighter lattice structure compared to the more symmetrically shaped Hiflow® ring packings. A tigher lattice structure might be preferable in terms of bubble inhibition that leads to more effective bubbling fluidization. However, the fuel conversion rates are equally high at higher bed heights.

Table 4.4 shows the pressure drop of a bed height when using RMSR, Hiflow® ring or no packings. According to the earlier experiments referenced in 2.2, the pressure drop is caused by particle hold- up, friction between the packings and gas, as well as friction between bed particles and the packings. For the experiments without packings, as there are no other known factors involved, the observed pressure drop is believed to be due to particle hold-up. Since the pressure drop is obtained only for the same bed heights and not for the same particle mass, this data cannot be directly compared. But it is likely that it is particle hold-up that affects the total bed pressure drop, rather than bubbles or friction between gas and packings.

5.3 Water-gas shift effect

From figure 4.1 it can be seen that the degree of improvement in fuel conversion rates for both Syngas and CO fuel are similar. The observed differences are not large enough to make any conclusions regarding this effect. Even if it is present, it is not the main factor for the improvement of fuel conversion rates. This is also supported by the conversion rate of H_2 shown in figure 4.3, where the rate is nearly 100% for all bed heights except 10 cm to 20 cm. The cause of the much lower conversion rate at the 10 and 15 cm bed heights is unknown. As was mentioned in section 2.5, the water-gas shift reaction is very weak and is even unlikely to take place without a catalyst. It is therefore unlikely that the reaction has any significant effect on the conversion rates.

5.4 Experiments with an empty bed

Table 4.6 indicates that there is some amount of CO_2 production and O_2 consumption. However, as it is less than 10 mass % of the oxygen per Ilmenite and the consumption is similar for both types of packings, it is deemed negligible. The CO_2 formation is the highest for the experiments without packings. This implies that the packings are not acting as oxygen carriers or catalysts in an oxidization process. Some possibles causes for the small amounts of O_2 consumption could be back mixing of air from the outlet of the reactor, small amounts of oxygen remaining in the reactor reacting with the fuel, or some part of the reactor taking part in the reaction, but it is impossible to draw any conclusions from the measured data. This effect should be the same for all set ups and therefore not of significance when comparing variables such as fuel, bed height or packing type.

5.5 Ilmenite quality control

The measured density of Ilmenite presented in table 4.5 indicates that the there is no significant difference between the samples before and after the Syngas experiments. Since Ilmenite has been proven to be sufficient in previous studies, and further study of the material itself was not within the project scope, more accurate testing was not conducted.

5.6 Limitations

This is an empirical study based on the observation of fuel conversion rates in relation to bed heights and different packing types. There are some nonoptimal conditions for the instruments used in the experiments, as well as for the data analysis. The data sets are small and the results should be seen as a general trend, not as statistically verified. Since there are only three or four data points for each configuration, and the analysis uses the average of these points, might not be accurate if there is a large variance in the measurements. As mentioned in section 3.2, the SICK sensor used is not originally intended to detect sudden changes in concentration and there is also a slight delay from when the flow rate is changed in the control software to when the gas is actually injected into the system. Entrainment was observed during the experiments, which was described in section 4.5. The amounts were considered negligible for this context but could be seen as a source of uncertainty.

A superficial gas velocity of 0.3 m/s was used in all experiments, regardless of bed height. Since the gas velocity could give different fluidization conditions, depending on the bed height and packings, this could affect the reaction in a way that complicates the comparison. Further research might be needed in this area. Another uncertainty lies in the randomness of the packing placement, especially with packings whose effects on flow are highly dependent on their placement direction, such as the Hiflow® ring, as they can affect the pressure drop and fluidization state as well as the reaction.

5.7 Future studies

A fuel conversion rate of nearly 100 % was reached with 60 cm bed heights but the difference between 55 cm and 60 cm was not large and some of the set ups, such as 55 cm, had higher fuel conversion rates than 60 cm. Industrial facilities are much larger than what is used in these experiments and for such applications it is important to know if this is a true trend, or if the observed drop in fuel conversion rate above 55 cm is due to measurement inaccuracies or other setup related issues, such as reactor size. Further research, using taller beds, is needed.

A study directly measuring the mass transfer rate could be useful for connecting the dots between fuel conversion rate, bubble inhibition and mass transfer rate. Understanding more about the formation and inhibition of bubbles in a fluidized

bed with packings will further connect the dots. This can be achieved through more detailed pressure and pressure drop analysis. Computational Fluid Dynamics(CFD) software could be a useful tool for the simulation and analysis of bubbles.

Even if it was found to not be an issue during these experiments, stainless steel packings can bring some uncertainty regarding oxidization and ash chemistry. Researching packings made from other materials would alleviate any such concerns. It would be also good doing more detailed research into the effects of different packing geometries. Finding an optimal shape and material for bubble inhibition and a optimized fluidization state in the reactor should be considered a major goal of further studies into the subject. It is also important to consider the effects on ash formation and packing lifetime, as both are important for industrial implementations. A temperature of 840 °C was set for the experiments in this study. The temperature can potentially affect the fluidization and reaction, and investigating systems with different combustion temperatures could be useful if other fuel types are to be considered. Other operational conditions worth study are effects related to pressure and furnace geometry.

6
Conclusions

The project experimentally investigated the fuel conversion rate improvement potential of using packings in a Chemical-Looping Combustion (CLC) fluidized bed reactor. The investigated variables are bed height, fuel type (Syngas and CO) and packing type (RMSR, Hiflow® ring or no packings). CLC provides inherent carbon capture advantages due to its easily separable flue gas but improvements in fuel conversion rates would provide an even more effective separation of CO_2, which in turn makes more effective Carbon capture and storage possible.

The key finding is that the use of packings lead to an increased fuel conversion rate for all tested bed heights and amounts of bed particles. Comparison of Hiflow® ring and RMSR packings indicate that the latter often is better but both provide significant improvements compared to the no packings test cases. For taller beds the improvement was similar for all tested packing types. Earlier studies indicate that the inhibition of large bubbles in a fludized bed reactor increases the mass-transfer rate and hence the fuel conversion rate. The tests conducted in this study support this idea. Observations of spillage as well as temperature and pressure fluctuations indicate the presence of large bubbles or slugging with taller bed heights when not using packings. RMSR packings seem to provide better bubble inhibition compared to Hiflow® ring, possibly because its geometry may allow it to form a tighter lattice structure. The fuel conversion rates generally increase with bed height, which could be due to the shorter reaction path as well as possible spouting with lower bed heights. Using packings, the absolute fuel conversion rate improvement is higher with lower beds but given that the conversion rate of tall beds without packings is already high to begin with, getting close to 100% with packings, the numbers are not easily comparable. Seen as a fraction of the theoretical maximum possible improvement at each bed height, the taller beds actually improve more than the lower beds when packings are used.

Investigating both Syngas and CO fuel shows that there is no significant difference in the fuel conversion rate between them. This leads to the conclusion that the water-gas shift reaction does not take place or only has a negligible effect.

There are various possible ways to move forward regarding future studies. Experiments with higher bed heights, different packing geometries, different packing materials and various operational conditions are all relevant subjects in regards to scaling up the technology for industrial applications. CFD analysis of the formation and inhibition of bubbles, as well as direct measurements of the mass transfer rate, are also interesting paths of inquiry.

Bibliography

[1] S. Anderson and R. Newell, "Prospects for Carbon Capture and Storage technologies", *Annual Review of Environment and Resources*, vol. 29, 2004.

[2] T. Gasser, C. Guivarch, K. Tachiiri, C. Jones, and P. Ciais, "Negative emissions physically needed to keepglobal warming below 2°C", *Nature Communications*, vol. 6, no. 7958, 2015.

[3] M. Bui, C. S. Adjiman, A. Bardw, E. J. Anthoyn, A. Boston, S. Brown, P. S. Fennell, S. Fuss, A. Galindo, L. A. Hackett, J. P. Hallett, H. J. Herzog, G. Jackson, J. Kemper, S. Krevor, G. C. Maitland, M. Matuszewski, I. S. Metcalfe, C. Petit, G. Puxty, J. Reimer, D. M. Reiner, E. S. Rubin, S. A. Scott, N. Shah, B. Smit, J. P. M. Trusler, P. Webley, J. Wilcoxx, and N. M. Dowell, "Carbon capture and storage (CCS): the way forward", *Energy Environmental Science*, vol. 11, 2018.

[4] S. S. M. Al-Fattah, M. F. Barghouty, B. O. D. Gaella Bureau, S. Fillacier, P. L. Thiez, C. McQuale, G. Munier, and J. Royer-Adnot, *Carbon Capture and Storage : Technologies, Policies, Economics, and Implementation Strategies*, 1st ed. Taylor Francis Group, 2011, p. 392, ISBN: 9780203123744.

[5] A. Lyngfelt, *"Chapter 20 Chemical Looping combustion (CLC)" in Fluidized bed technologies for near-zero emission combustion and gasification*, 1st ed. Woodhead Publishing Limited, 2013, pp. 895–930, ISBN: 9780857095411.

[6] A. Lyngfelt and C. Linderholm, "Chemical-Looping Combustion of Solid Fuels – status and recent progress", *Energy Procedia*, 2017.

[7] A. Lyngfelt and B. Leckner, "A 1000 MWth boiler for chemical-looping combustion of solid fuels – Discussion of design and costs", *Applied Energy*, vol. 157, 2015.

[8] A. Lyngfelt, A. Brink, Øyvind Langørgen, T. Mattisson, M. Rydén, and C. Linderholm, "11,000 h of chemical-looping combustion operation—Where are we and where do we want to go?", *International Journal of Greenhouse Gas Control*, vol. 88, 2019.

[9] A. Lyngfelt, "Chemical Looping Combustion: Status and Development Challenges", *Energy Fuels*, vol. 34, 2020.

[10] ——, *Calcium and Chemical Looping Technology for Power Generation and Carbon Dioxide (CO2) Capture*, P. Fennell and B. Anthony, Eds. In Woodhead Publishing, 2015.

[11] J. Aronsson, D. Pallarès, and A. Lyngfelt, "Modeling and scale analysis of gaseous fuel reactors in chemical looping combustion systems", *Particuology*, vol. 35, 2017.

[12] J. Aronsson, D. Pallarès, M. Rydén, and A. Lyngfelt, "Increasing Gas–Solids Mass Transfer in Fluidized Beds by Application of Confined Fluidization—A Feasibility Study", *applied science*, vol. 9, no. 634, 2019.

[13] J. Aronsson, E. Krymarys, V. Stenberg, T. Mattisson, A. Lyngfelt, and M. Rydén, "Improved Gas-Solids Mass Transfer in Fluidized Beds: Confined Fluidization in Chemical-Looping Combustion", *Energy fuels*, vol. 33, no. 5, pp. 4442–4453, 2019.

[14] L.-S. Fan, *Chemical Looping Technology and Its Fossil Energy Conversion Applications*. John Wiley Sons, 2010.

[15] D. Kunii and O. Levenspiel, *Fluidization engineering*, 2nd ed. Butterworth Heinemann, 1991.

[16] D. Geldart, "Types of Gas Fulidization", *Power technology*, vol. 7, 1973.

[17] M. Rhodes, *Particle technology*, 2nd ed. John Wiley Sons,Ltd, 2008.

[18] J. R. Grace, "Contacting Modes and Behaviour classification of Gas-Solid and Other Two-Phase Suspension ", *The Canadian journal of chemical engineering*, vol. 64, 1986.

[19] J. Sutherland, G. Vassilatos, and a. G. L. O. Hiroshi Kubota, "The Effect of Packing on a Fluidized Bed", *American Institute of Chemical Engineers*, vol. 9, no. 4, pp. 437–441, 1963.

[20] R. G. Holdich, *Fundamentals of Particle Technology*. Midland Information Technology Publishing, 2002.

[21] G. Donsi, G. Ferrari, and B. Formisani, "Expansion Behaviour of Confined Fluidized Beds of Fine Particles", *The Canadian journal of chemical engineering*, vol. 67, 1989.

[22] X. Song, Z. Wang, Y. Jin, and Z. Tanaka, "Gas-solids circulating fluidization in a packed bed", *Powder Technology*, vol. 83, 1995.

[23] K. Allen, T. von Backström, and D. Kröger, "Packed bed pressure drop dependence on particle shape, size distribution, packing arrangement and roughness", *Powder Technology*, vol. 246, 2013.

[24] T. Chinba and H. Kobayashi, "Gas exchange between the bubble and emulsion phases in gas-solid fluidized beds", *Chemical Engineering Science,*, vol. 25, 1970.

[25] Z. Fu, J. Zhu, S. Barghi, Y. Zhao, Z. Luo, and C. Duan, "On the two-phase theory of fluidization for Geldart B and D particles", *Chemical Engineering Science*, vol. 345, 2019.

[26] H. Leion, V. Frick, and F. Hildor, "Experimental Method and Setup for Laboratory Fluidized Bed Reactor Testing", *International Journal of Greenhouse Gas Control*, vol. 11, no. 2505, 2018.

[27] W.-H. Chena and C.-Y. Chen, "Water gas shift reaction for hydrogen production and carbon dioxide capture: A review", *Applied Energy*, vol. 258, 2020.

[28] B. Smith, L. Muruganandam, and S. Shantha, "A Review of the Water Gas Shift Reaction Kinetics", *International Journal of Chemical Reactor Engineering*, vol. 8, 2010.

[29] G. Schwebel, H. Leion, and W. Krumm, "Comparison of natural ilmenites as oxygen carriers in chemical-looping combustion and influence of water gas shift

reaction on gas composition", *Chemical Engineering Research and Design*, vol. 90, no. 9, 1351—1360, 2012.

[30] J. Highley, *"Chapter 5 Fluidized-bed combustion" in The Efficient Use of Energy*, 2nd ed., J. Dryden, Ed. Elsevier Ltd, 1982, pp. 53–63.

[31] (2017). Heat of combustion, Engineering ToolBox, [Online]. Available: `https://www.engineeringtoolbox.com/standard-heat-of-combustion-energy-content-d_1987.html` (visited on 11/29/2020).

A

Appendix I

A.1 Measurements of mass for Ilmenite, packings and packing void

Repetition	Before [g]	After [g]
1	41.0	42.5
2	40.8	41.3
3	41.8	40.9
4	41.1	40.8
5	41.0	41.3
6	40.8	40.6
7	40.6	41.1
8	41.2	40.9
9	41.2	40.3
10	41.4	41.9
Average	41.1	41.2

Table A.1: Ilmenite mass measured before and after Syngas experiments.

Repetition	RMSR [g]	Hiflow [g]
1	962.2	953.7
2	959.9	939.3
3	950.1	947.1
4	957.3	952.2
Average	957	948

Table A.2: Measured water mass occupying the packing void.

Repetition	RMSR [g]	Hiflow [g]
1	191.0	264.3
2	190.7	274.0
3	198.5	273.9
4	200.1	273.7
Average	195.0	271.5

Table A.3: Measured packing mass.

A.2 Fuel conversion rate versus Ilmenite oxygen conversion rate

A.2.1 Syngas fuel experiments

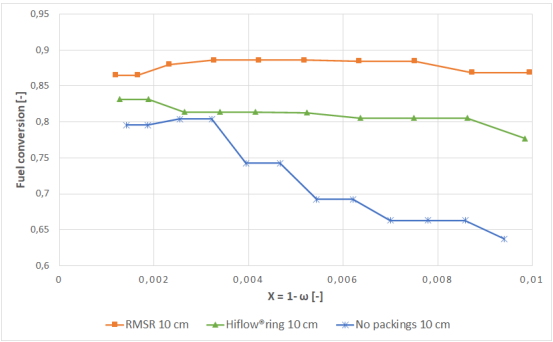

Figure A.1: Fuel conversion rate versus Ilmenite oxygen conversion rate using Syngas fuel, 10 cm bed height.

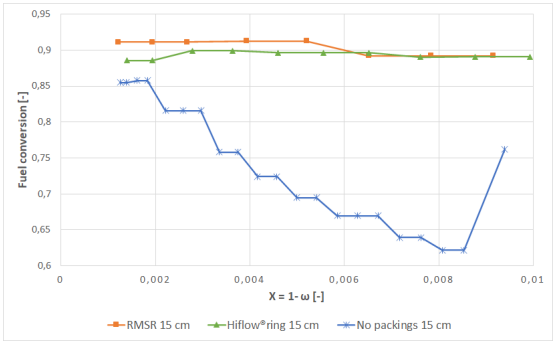

Figure A.2: Fuel conversion rate versus Ilmenite oxygen conversion rate using Syngas fuel, 15 cm bed height.

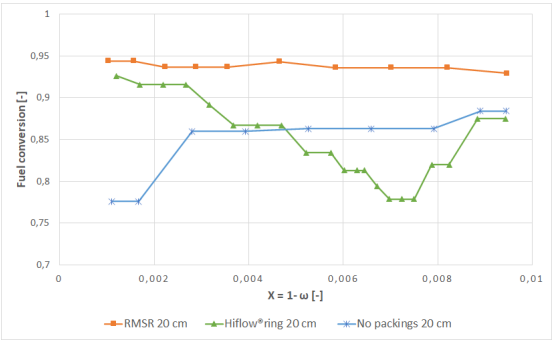

Figure A.3: Fuel conversion rate versus Ilmenite oxygen conversion rate using Syngas fuel, 20 cm bed height.

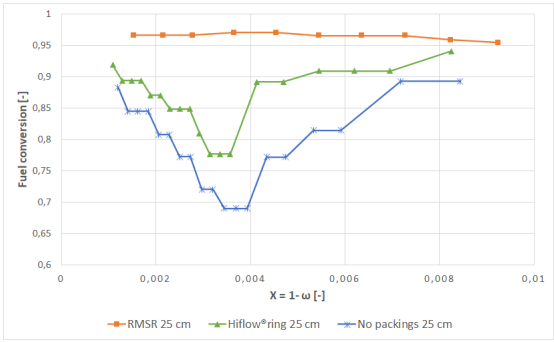

Figure A.4: Fuel conversion rate versus Ilmenite oxygen conversion rate using Syngas fuel, 25 cm bed height.

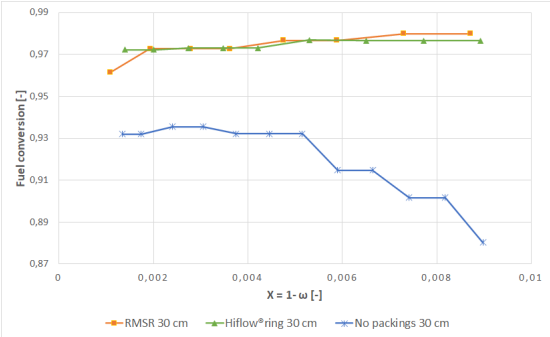

Figure A.5: Fuel conversion rate versus Ilmenite oxygen conversion rate using Syngas fuel, 30 cm bed height.

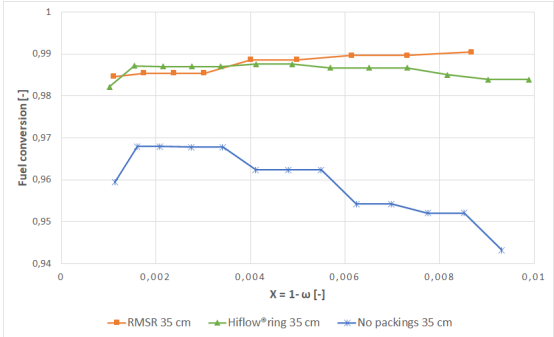

Figure A.6: Fuel conversion rate versus Ilmenite oxygen conversion rate using Syngas fuel, 35 cm bed height.

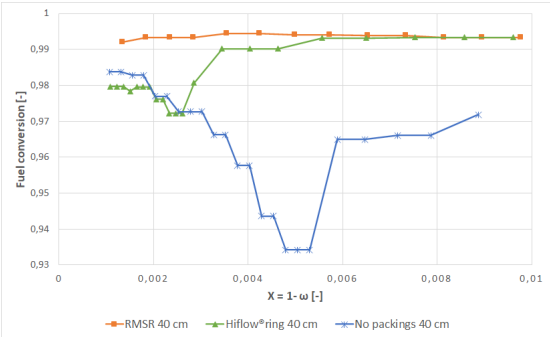

Figure A.7: Fuel conversion rate versus Ilmenite oxygen conversion rate using Syngas fuel, 40 cm bed height.

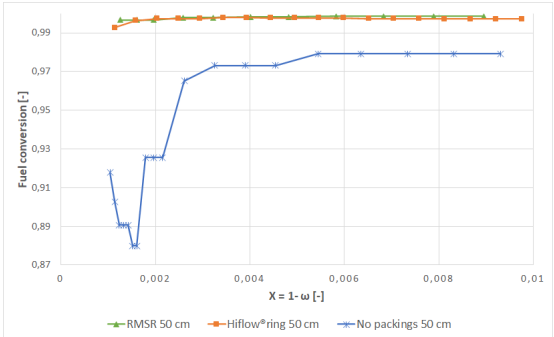

Figure A.8: Fuel conversion rate versus Ilmenite oxygen conversion rate using Syngas fuel, 50 cm bed height.

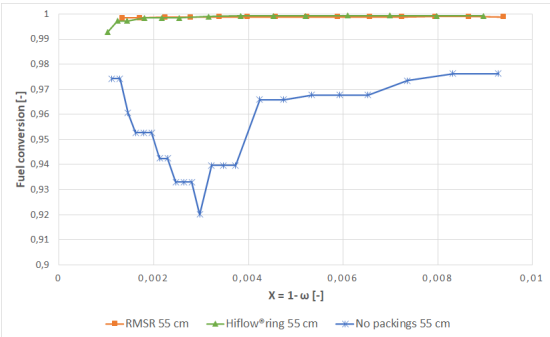

Figure A.9: Fuel conversion rate versus Ilmenite oxygen conversion rate using Syngas fuel, 55 cm bed height.

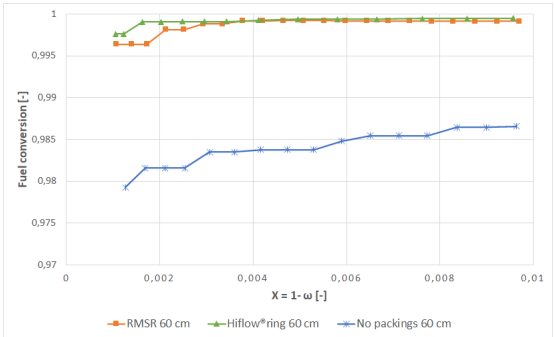

Figure A.10: Fuel conversion rate versus Ilmenite oxygen conversion rate using Syngas fuel, 60 cm bed height.

A.2.2 CO fuel experiments

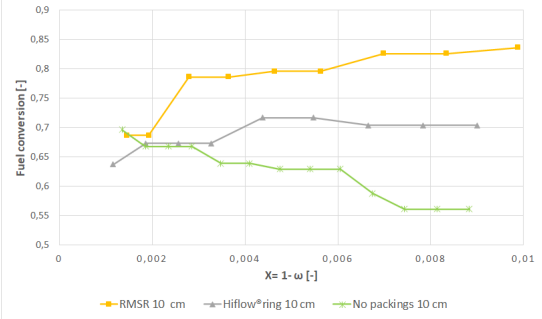

Figure A.11: Fuel conversion rate versus Ilmenite oxygen conversion rate using CO fuel, 10 cm bed height.

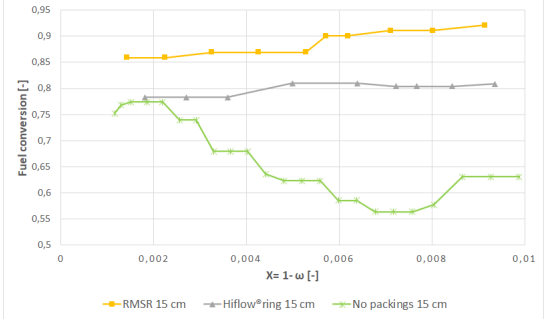

Figure A.12: Fuel conversion rate versus Ilmenite oxygen conversion rate using CO fuel, 15 cm bed height.

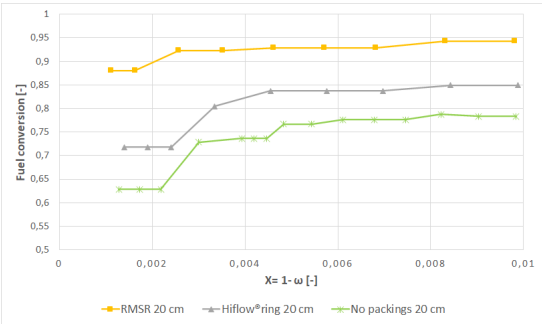

Figure A.13: Fuel conversion rate versus Ilmenite oxygen conversion rate using CO fuel, 20 cm bed height.

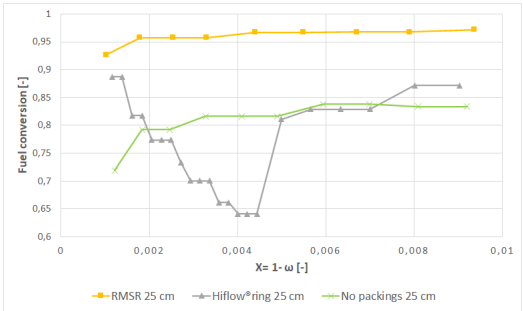

Figure A.14: Fuel conversion rate versus Ilmenite oxygen conversion rate using CO fuel, 25 cm bed height.

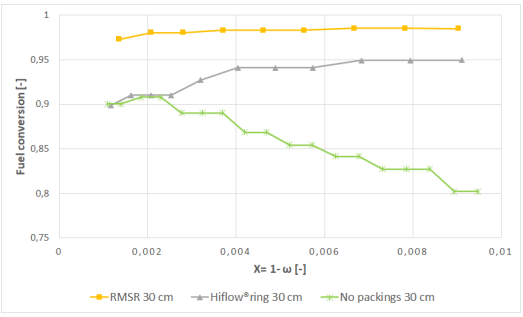

Figure A.15: Fuel conversion rate versus Ilmenite oxygen conversion rate using CO fuel, 30 cm bed height.

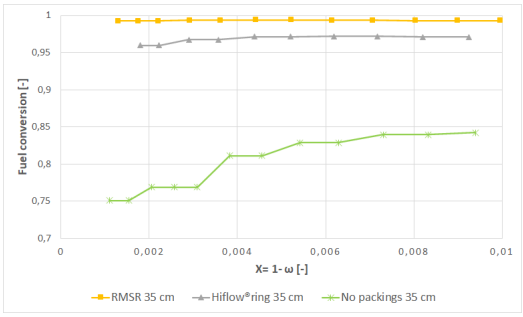

Figure A.16: Fuel conversion rate versus Ilmenite oxygen conversion rate using CO fuel, 35 cm bed height.

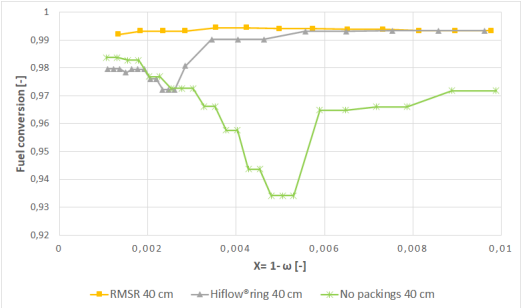

Figure A.17: Fuel conversion rate versus Ilmenite oxygen conversion rate using CO fuel, 40 cm bed height.

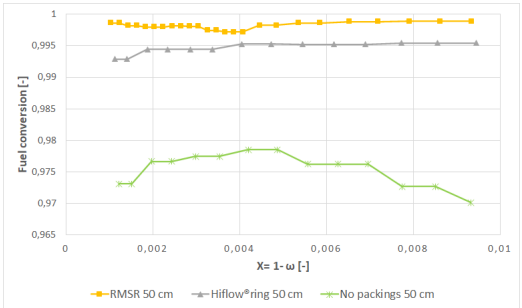

Figure A.18: Fuel conversion rate versus Ilmenite oxygen conversion rate using CO fuel, 50 cm bed height.

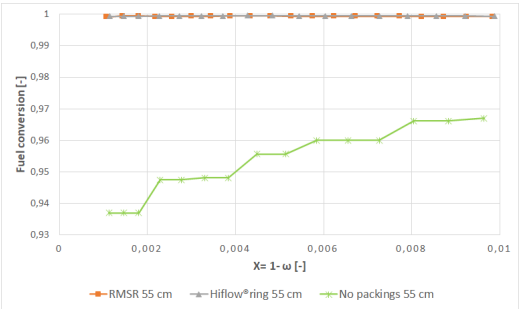

Figure A.19: Fuel conversion rate versus Ilmenite oxygen conversion rate using CO fuel, 55 cm bed height.

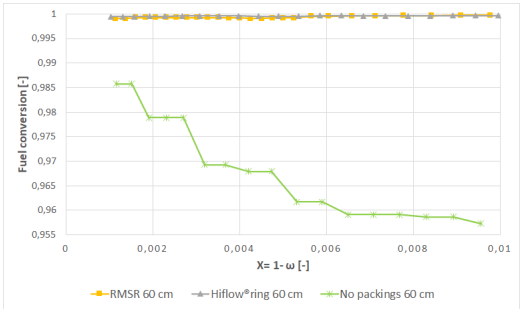

Figure A.20: Fuel conversion rate versus Ilmenite oxygen conversion rate using CO fuel, 60 cm bed height.

A.3 Temperature

A.3.1 Syngas experiments

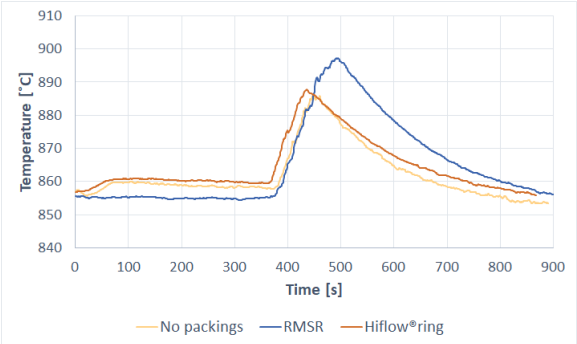

Figure A.21: Temperature change over time using Syngas fuel, 15 cm bed height and RMSR, Hiflow® ring or no packings.

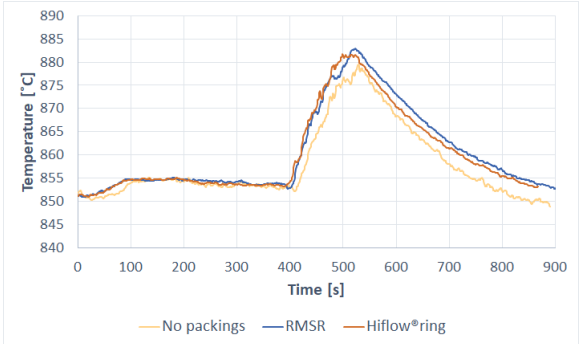

Figure A.22: Temperature change over time using Syngas fuel, 25 cm bed height and RMSR, Hiflow® ring or no packings.

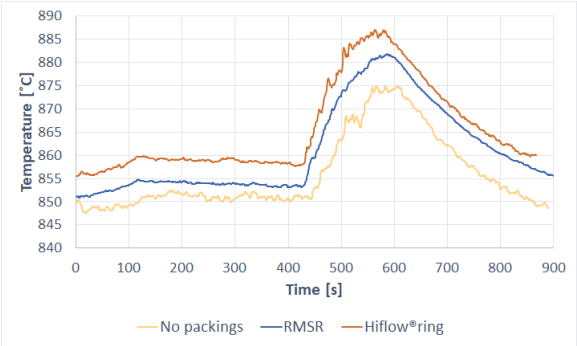

Figure A.23: Temperature change over time using Syngas fuel, 35 cm bed height and RMSR, Hiflow® ring or no packings.

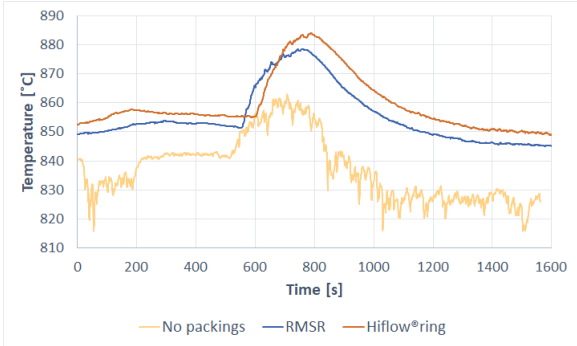

Figure A.24: Temperature change over time using Syngas fuel, 55 cm bed height and RMSR, Hiflow® ring or no packings.

A.3.2 CO experiments

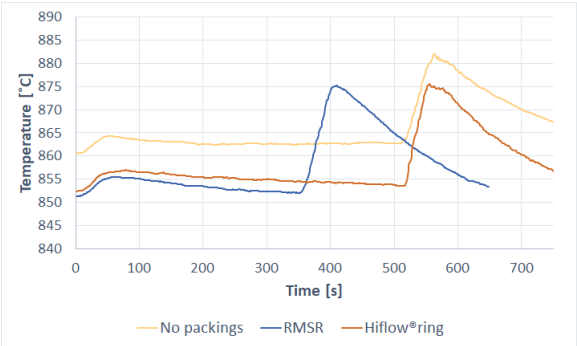

Figure A.25: Temperature change over time using CO fuel, 10 cm bed height and RMSR, Hiflow® ring or no packings.

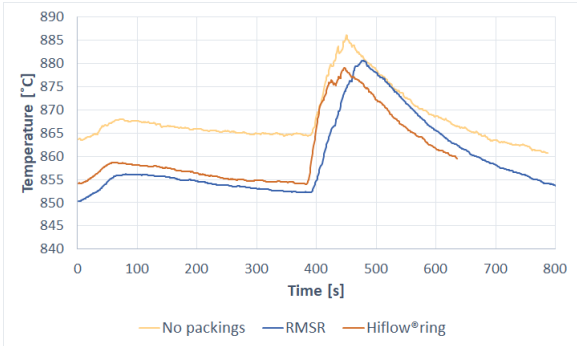

Figure A.26: Temperature change over time using CO fuel, 15 cm bed height and RMSR, Hiflow® ring or no packings.

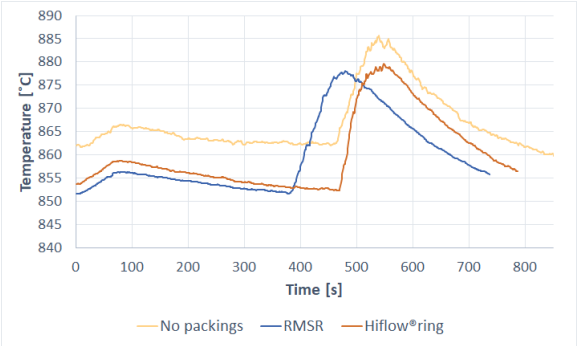

Figure A.27: Temperature change over time using CO fuel, 20 cm bed height and RMSR, Hiflow® ring or no packings.

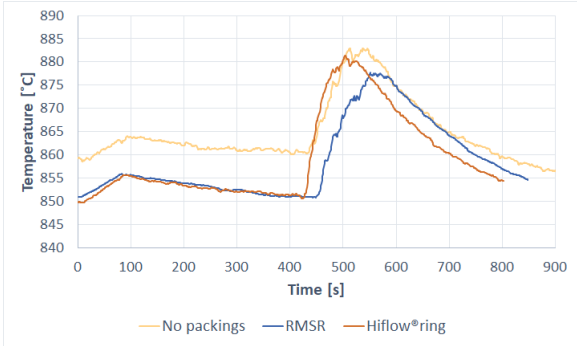

Figure A.28: Temperature change over time using CO fuel, 25 cm bed height and RMSR, Hiflow® ring or no packings.

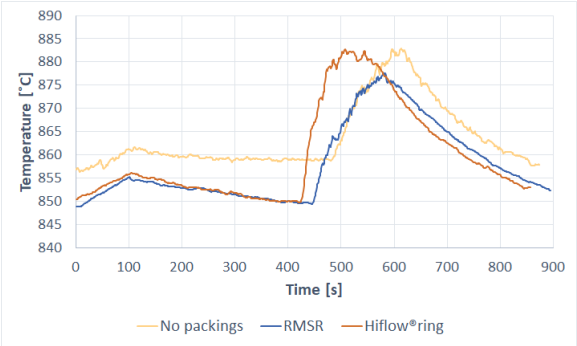

Figure A.29: Temperature change over time using CO fuel, 30 cm bed height and RMSR, Hiflow® ring or no packings.

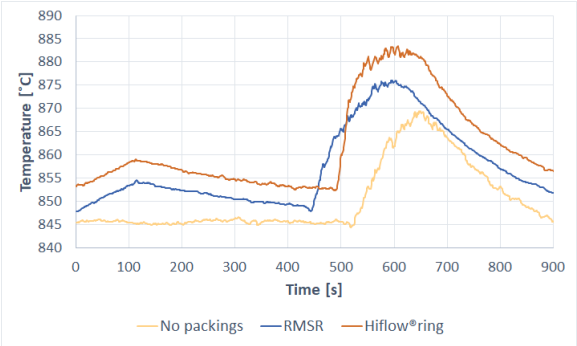

Figure A.30: Temperature change over time using CO fuel, 35 cm bed height and RMSR, Hiflow® ring or no packings.

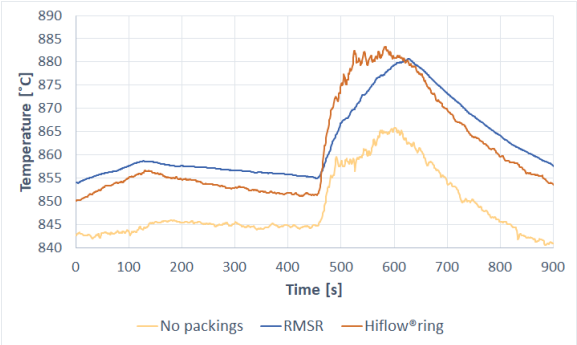

Figure A.31: Temperature change over time using CO fuel, 40 cm bed height and RMSR, Hiflow® ring or no packings.

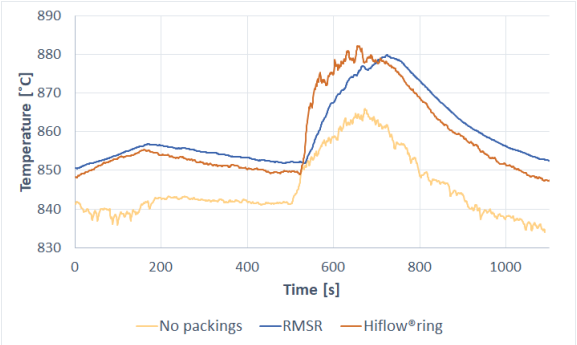

Figure A.32: Temperature change over time using CO fuel, 50 cm bed height and RMSR, Hiflow® ring or no packings.

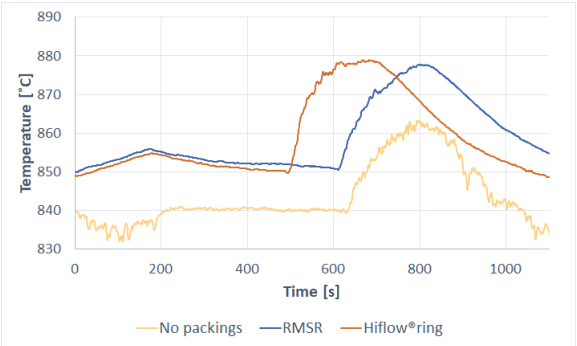

Figure A.33: Temperature change over time using CO fuel, 55 cm bed height and RMSR, Hiflow® ring or no packings.

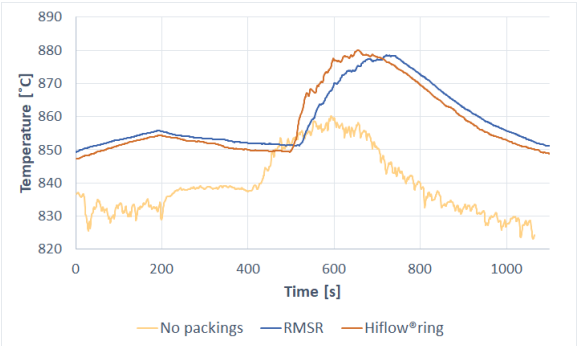

Figure A.34: Temperature change over time using CO fuel, 60 cm bed height and RMSR, Hiflow® ring or no packings.

A.4 Pressure

A.4.1 Syngas experiments

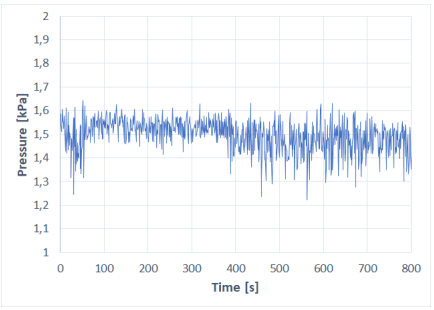

(a) No packings

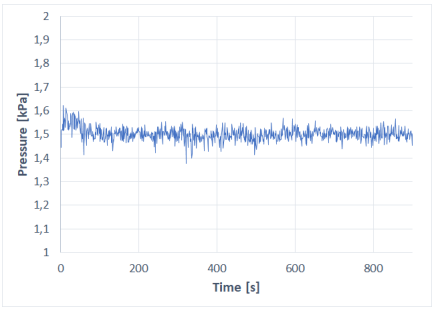

(b) RMSR

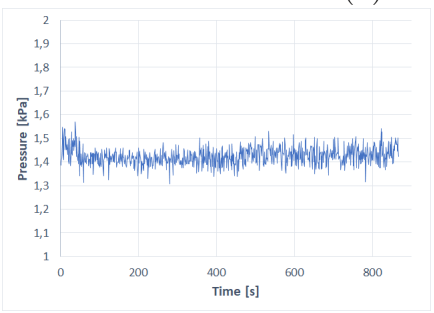

(c) Hiflow® ring

Figure A.35: Pressure comparison for 15 cm bed height, Syngas fuel and using RMSR, Hiflow® ring or no packings

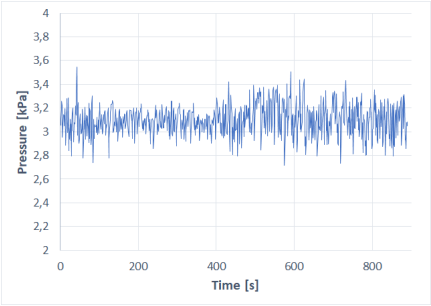

(a) No packings

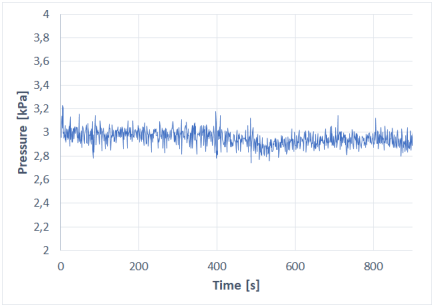

(b) RMSR

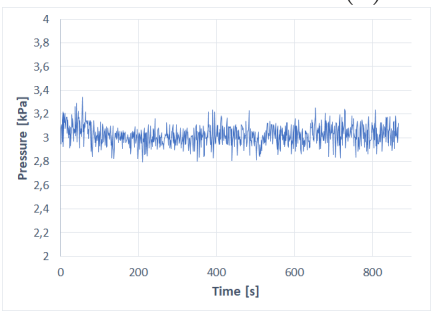

(c) Hiflow® ring

Figure A.36: Pressure comparison for 25 cm bed height, Syngas fuel and using RMSR, Hiflow® ring or no packings

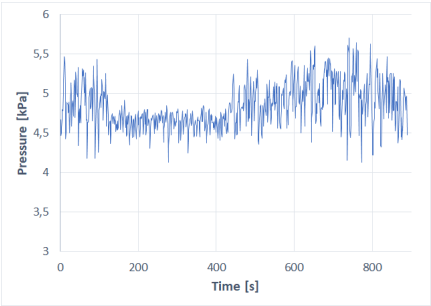

(a) No packings

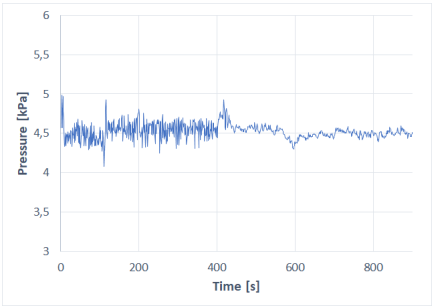

(b) RMSR

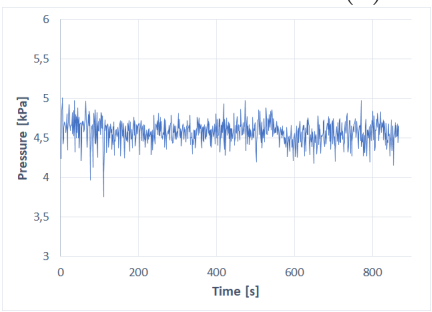

(c) Hiflow® ring

Figure A.37: Pressure comparison for 35 cm bed height, Syngas fuel and using RMSR, Hiflow® ring or no packings

A.4.2 CO experiments

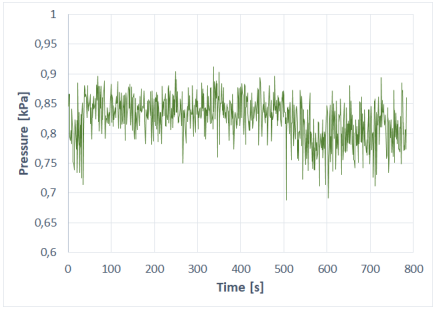

(a) No packings

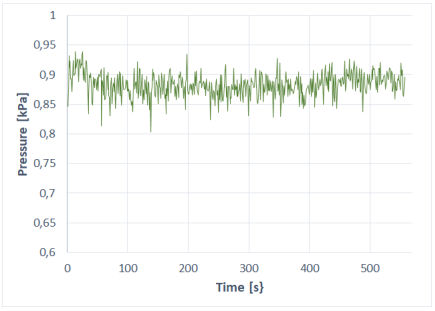

(b) RMSR

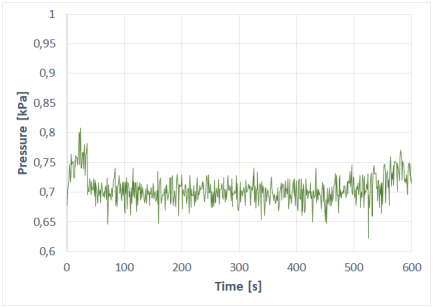

(c) Hiflow® ring

Figure A.38: Pressure comparison for 10 cm bed height, CO fuel and using RMSR, Hiflow® ring or no packings

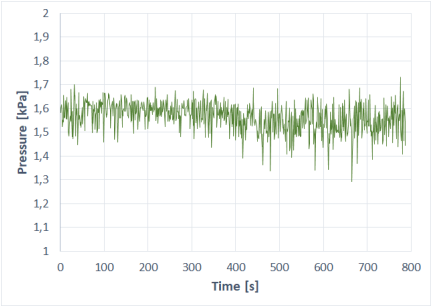

(a) No packings

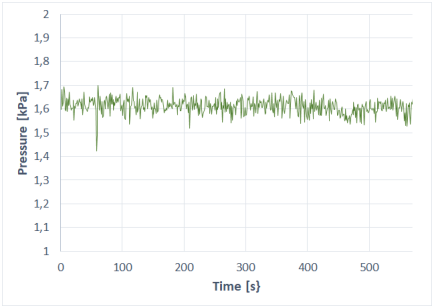

(b) RMSR

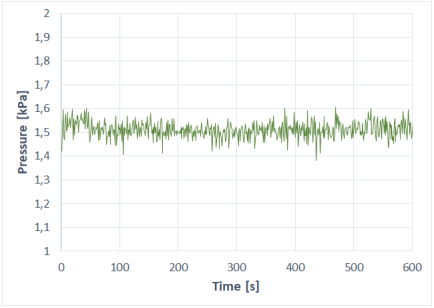

(c) Hiflow® ring

Figure A.39: Pressure comparison for 15 cm bed height, CO fuel and using RMSR, Hiflow® ring or no packings

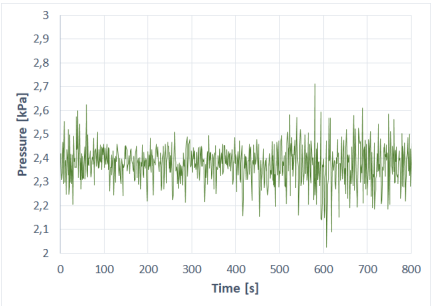

(a) No packings

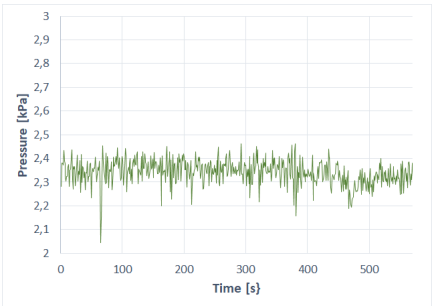

(b) RMSR

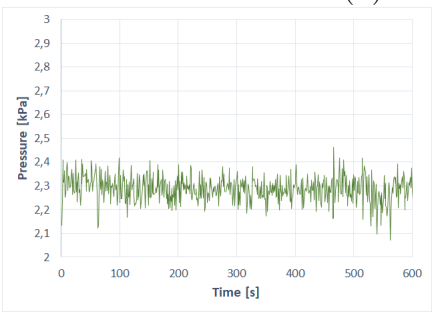

(c) Hiflow® ring

Figure A.40: Pressure comparison for 20 cm bed height, CO fuel and using RMSR, Hiflow® ring or no packings

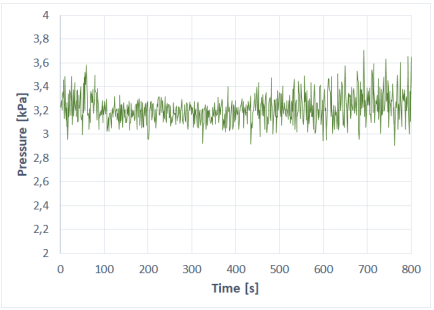

(a) No packings

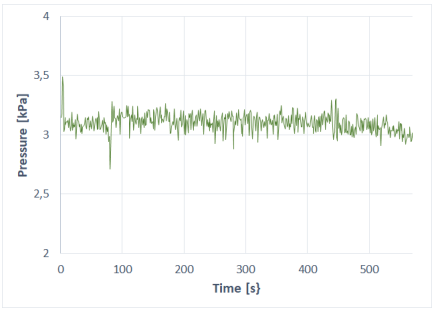

(b) RMSR

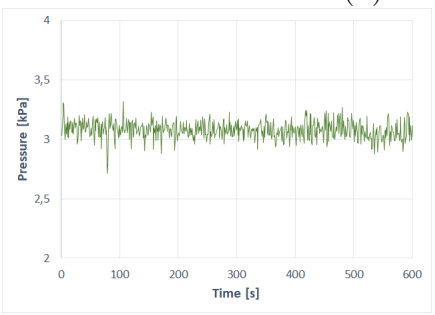

(c) Hiflow® ring

Figure A.41: Pressure comparison for 25 cm bed height, CO fuel and using RMSR, Hiflow® ring or no packings

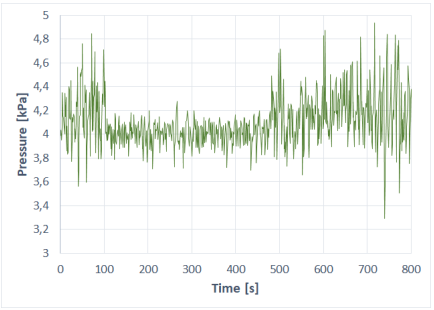

(a) No packings

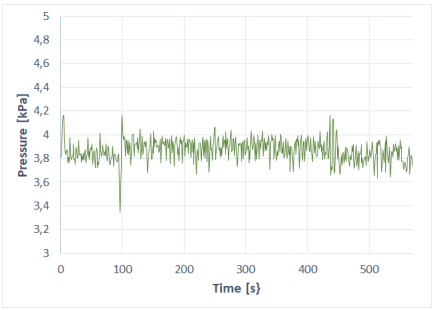

(b) RMSR

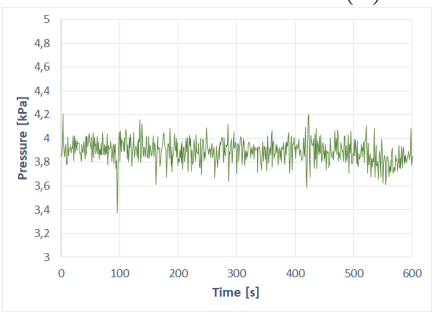

(c) Hiflow® ring

Figure A.42: Pressure comparison for 30 cm bed height, CO fuel and using RMSR, Hiflow® ring or no packings

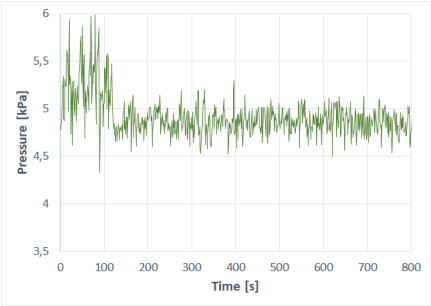

(a) No packings

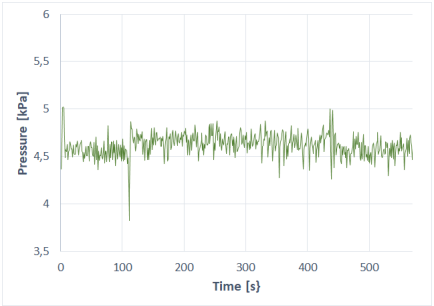

(b) RMSR

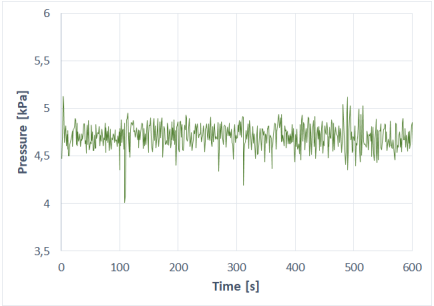

(c) Hiflow® ring

Figure A.43: Pressure comparison for 35 cm bed height, CO fuel and using RMSR, Hiflow® ring or no packings

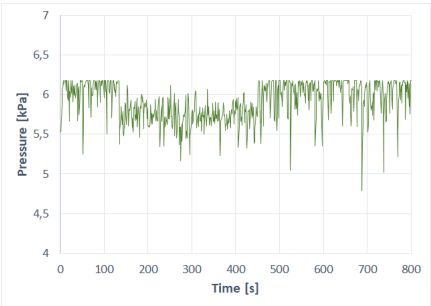

(a) No packings

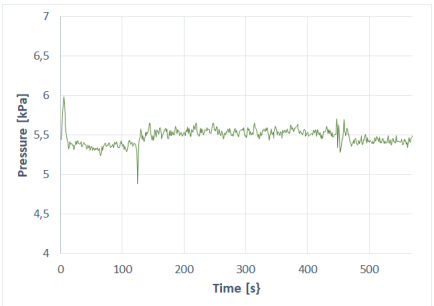

(b) RMSR

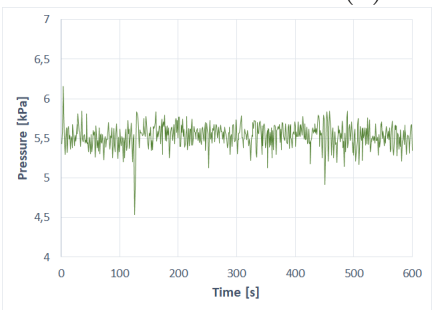

(c) Hiflow® ring

Figure A.44: Pressure comparison for 40 cm bed height, CO fuel and using RMSR, Hiflow® ring or no packings